Redox Biology 58 (2022) 102546

Contents lists available at ScienceDirect

Redox Biology

journal homepage: www.elsevier.com/locate/redox

HDLBP-stabilized lncFAL inhibits ferroptosis vulnerability by diminishing Trim69-dependent FSP1 degradation in hepatocellular carcinoma

Jingsheng Yuan [a,b,1], Tao Lv [a,b,1], Jian Yang [a,b,1], Zhenru Wu [c], Lvnan Yan [a,b], Jiayin Yang [a,b,*], Yujun Shi [b,c,**]

[a] Department of Liver Surgery and Liver Transplantation Center, West China Hospital of Sichuan University, Chengdu, 610041, China
[b] Laboratory of Liver Transplantation, Frontiers Science Center for Disease-related Molecular Network, West China Hospital of Sichuan University, Chengdu, 610041, China
[c] Laboratory of Pathology, Key Laboratory of Transplant Engineering and Immunology, NHC, West China Hospital of Sichuan University, Chengdu, 610041, China

ARTICLE INFO

Keywords:
Hepatocellular carcinoma
Ferroptosis
HDLBP
lncRNA
FSP1
Ubiquitination

ABSTRACT

Recent studies have suggested that exploring the potential mechanisms regulating ferroptosis vulnerability may contribute to improving the systemic therapeutic efficacy in HCC. High-density lipoprotein-binding protein (HDLBP), the largest RNA-binding protein, is an important transporter that protects cells from overaccumulation of cholesterol, but few studies have elucidated the role of HDLBP in the regulation of ferroptosis vulnerability in HCC. Our study suggests that HDLBP was markedly elevated in HCC compared with noncancerous liver tissues and that this elevation inhibited the ferroptosis vulnerability of HCC. Further experiments revealed that HDLBP bound to and stabilized the long noncoding RNA lncFAL (ferroptosis-associated lncRNA), which is derived from the plexin B2 gene. Moreover, our study suggests that the splicing of lncFAL was increased by YTH N6-methyladenosine (m6A) RNA-binding protein 2 (YTHDF2) in a m6A-dependent manner. Although HDLBP or lncFAL could not regulate the GPX4 antioxidant signalling pathway, lncFAL reduced ferroptosis vulnerability by directly binding to ferroptosis suppressor protein 1 (FSP1) and competitively abolishing Trim69-dependent FSP1 polyubiquitination degradation. More importantly, FSP1 inhibition promoted the antitumour activity of ferroptosis inducers both *in vitro* and *in vivo*. Collectively, our results provide a clinically promising demonstration that HDLBP stabilizes lncFAL, which mediates a FSP1-dependent anti-ferroptosis mechanism in HCC. These results support the enormous potential of disrupting FSP1 as a promising therapeutic approach for HCC patients with high HDLBP or lncFAL expression.

1. Introduction

Although the causative factors for hepatocellular carcinoma (HCC) have been identified and preventive strategies such as hepatitis vaccines, avoidance of alcohol, and excessive obesity have been routinely recommended in clinical practice [1,2], statistics indicate that the global burden of HCC is still increasing [3]. Recent data suggest that 40–50% of HCC patients are diagnosed early due to disease surveillance programs and are eligible for potential curative therapy, but almost half of all HCC patients eventually receive systemic therapy [4]. In recent years, landmark advances have been made in the systemic treatment of HCC [5]. Sorafenib, the first multikinase inhibitor approved by the FDA for the treatment of HCC, has improved the median overall survival (OS) time of HCC patients from 7.9 months to 10.7 months [6]. Several other new drugs, including the first-line drug lenvatinib and the second-line drugs regorafenib and cabozantinib, have also exhibited some clinical benefit [7,8], but clinical statistics suggest that the median OS of HCC patients remains approximately 1 year [9]. Since 2020, immune checkpoint inhibitors have been incorporated into HCC treatment regimens, and the combination of targeted therapies with immunotherapy is emerging as the most promising clinical treatment option for HCC [10]. However, the improvement in HCC patient prognosis remains limited. Therefore,

* Corresponding author. Department of Liver Surgery and Liver Transplantation Center, West China Hospital of Sichuan University, Chengdu, 610041, China.
** Corresponding author. Laboratory of Liver Transplantation, Frontiers Science Center for Disease-related Molecular Network, West China Hospital of Sichuan University, Chengdu, 610041, China.
E-mail addresses: doctoryjy@scu.edu.cn (J. Yang), shiyujun@scu.edu.cn (Y. Shi).
[1] These authors contributed equally to this work.

https://doi.org/10.1016/j.redox.2022.102546
Received 5 October 2022; Received in revised form 10 November 2022; Accepted 16 November 2022
Available online 19 November 2022

novel therapeutic targets for HCC still need to be identified to improve the survival outcome of patients with this disease.

Ferroptosis is a newly proposed mechanism of programmed cell death that occurs in response to ATP production but is independent of caspase activation [11]. Although many small molecules have been found to induce ferroptosis in various cancer cells, ferroptosis is insensitive to the inhibition of cyclophilin D (a necrosis inhibitor) or 3-methyladenine (an autophagy inhibitor) [12]. The main mechanisms of ferroptosis include the disruption of iron homeostasis and the destruction of redox homeostasis [11]. Among these mechanisms, intracellular redox homeostasis is mainly regulated by the glutamine/GPX4 metabolic pathway and the ferroptosis suppressor protein 1 (FSP1)/CoQ10/NAP(D)H pathway [13]. Given the nonapoptotic feature of ferroptosis, ferroptosis-based tumour therapies might bypass traditional apoptosis-mediated cell death mechanisms to exert tumour suppressive effects. However, distinct types of tumours appear to exhibit varying vulnerability to ferroptosis [13]. Recent studies have reported that T cells and interferon-gamma can sensitize tumour cells to ferroptosis [14], which makes targeting ferroptosis in combination with cancer immunotherapy a promising strategy. Moreover, systemic therapeutic agents for HCC, such as sorafenib and lenvatinib, can partially exert antitumour efficacy by inducing ferroptosis [15,16]. These findings emphasize that exploring the potential mechanisms regulating ferroptosis vulnerability may contribute to improving the systemic therapeutic efficacy in HCC.

Abnormal cholesterol metabolism has been demonstrated to play an increasingly important role in cancer progression by providing energy and by macromolecular and cholesterol-mediated signalling [17]. The occurrence and development of many benign and malignant liver diseases, including HCC, are associated with abnormal cholesterol metabolism [18]. High-density lipoprotein-binding protein (HDLBP), also known as vigilin, plays an essential role in protecting cells against excessive cholesterol accumulation. Moreover, HDLBP is the largest RNA-binding protein and regulates transcription and translation by binding to RNA or single-stranded DNA [19]. Previous studies indicate that elevated HDLBP expression promotes cell proliferation and metastasis in HCC [20]. However, the potential roles of HDLBP in ferroptosis vulnerability remain incompletely investigated in HCC.

In this study, we found that elevated HDLBP expression inhibited ferroptosis vulnerability by binding to the cytoplasmic lncRNA lncFAL (ferroptosis-associated lncRNA) in HCC. Moreover, we further elucidated the critical role of lncFAL in ferroptosis vulnerability and its regulatory mechanisms. More importantly, our study indicates that FSP1 blockade may be a promising therapeutic strategy for HCC patients with high expression levels of HDLBP and lncFAL.

2. Materials and methods

2.1. Clinical samples

A retrospective analysis of HCC patients who underwent curative surgery at West China Hospital of Sichuan University was performed from June 2013 to December 2018. Sixty HCC tissues and 30 paired noncancerous liver (NCL) tissues were obtained from West China Biobanks. The clinicopathological diagnosis of HCC was confirmed for all the samples through pathology reports. This study using clinical samples was approved by the Ethics Committee on Biomedical Research, West China Hospital of Sichuan University (2016, no. 120). All patients provided written informed consent in line with the Declaration of Helsinki.

2.2. Cell culture and reagents

Human HCC cell lines (HepG2, Huh7, PLC5, SUN387 and Hep3B) were purchased from the Cell Bank of the Chinese Academy of Sciences (Shanghai, China). Human LO2 cells were obtained from Shi et al. [21]. All cell lines were cultured in DMEM (Gibco, NY, USA) supplemented with 10% foetal bovine serum (FBS) (ScienCell, CA, USA) and 1% penicillin and streptomycin (HyClone, UT, USA) and grown at 37 °C in humidified air with 5% CO_2. All cell lines were analysed by short tandem repeat profiling for cell line authentication and routine mycoplasma detection. Sorafenib-adapted culture of HCC cells was performed according to our previously published method [22].

Erastin (S7242), sorafenib (S7397), RSL3 (S8155), Z-VAD-FMK (S7023), actinomycin D (ActD, S8964), and MG132 (S2619) were purchased from Selleck (Houston, TX, USA). Ferrostatin-1 (Fer-1, HY100579) was procured from MedChemExpress (Shanghai, China). The RNase inhibitor RNasin (R0102) and DEPC (R0021) were purchased from Beyotime (Wuhan, China). Ubiquinol was obtained from Merck (992-78-9, Darmstadt, Germany).

2.3. RNA sequencing and bioinformatics

Total RNA was extracted from the cells using a TRIzol kit (Takara, Dalian, China). Transcriptome sequencing and subsequent data analysis were performed by Novogene (Tianjin, China). R 4.1.3 was used for the bioinformatics analysis. The R 'limma' package was used to identify differentially expressed genes between the indicated groups based on the following criteria: false discovery rate<0.05 and |log2 (fold change (FC))|>1. Gene set enrichment analysis (GSEA) and gene set variation analysis (GSVA) were performed to determine which Gene Ontology (GO) categories were enriched in the differential characteristic gene sets between the indicated groups. Liver hepatocellular carcinoma (LIHC) data from The Cancer Genome Atlas (TCGA) and indicated HCC datasets from the Gene Expression Omnibus (GEO) database were used to validate the expression levels of the target genes. The Vienna RNAfold web server (http://rna.tbi.univie.ac.at) was used to predict the secondary structure of lncFAL with minimum free energy. The online BioGRID (https://thebiogrid.org) and IntAct (https://www.ebi.ac.uk/legacy-intact/) databases were used for the analysis of protein–protein binding. Potential RNA methylation sites were analysed using the online SRAMP (http://www.cuilab.cn/sramp/) database. The online lncPro (http://bioinfo.bjmu.edu.cn/lncpro/) database was used for the prediction of lncRNA−protein interactions.

2.4. Cell viability assay

Cell viability was evaluated using a cell counting kit-8 (CCK-8) (AR1199, BOSTER, Wuhan, China) according to the manufacturer's instructions. Briefly, the processed cells (1×10^3 per well) were inoculated in 96-well plates for 24 h. Treatment with erastin or RSL3 for indicated time or sorafenib for 72 h was then performed according to the indicated concentrations. CCK-8 solution (10 μl) was added to each well, and the plate was incubated for 2 h. The absorbance at 450 nmol was then analysed and calculated.

In addition, to directly analysis the survival status of the HCC cells, Calcein-AM/PI staining assays were performed using an Calcein/PI Cell Viability/Cytotoxicity Assay Kit (Beyotime, C2015S, Wuhan, China) in accordance with the manufacturer's instructions.

2.5. Assessment of ferroptosis

To assess the level of ferroptosis in HCC cells after drug treatment, we assessed the levels of reactive oxygen species (ROS), lipid peroxidation, and mitochondrial damage in cells. Specifically, the ROS levels were assessed using a Reactive Oxygen Species Assay Kit (Beyotime, S0033S, Wuhan, China) in accordance with the manufacturer's instructions. The lipid peroxidation level was assessed using a C11-BODIPY Reagent Set (Thermo Fisher Scientific, 2115250, WI, USA) in accordance with the manufacturer's instructions. Mitochondrial damage was assessed using an enhanced mitochondrial membrane potential assay kit with JC-1 (Beyotime, C2003S, Wuhan, China) in accordance with the manufacturer's instructions. In addition, HCC cells were assessed by fluorescence

microscopy (Zeiss, Oberkochen, Germany) to analyse the degree of ferroptosis in cells treated with the indicated drugs.

2.6. RNA extraction and quantitative real-time polymerase chain reaction (qRT–PCR)

qRT–PCR was performed as described previously [22]. The primer sequences used for qRT–PCR are shown in Table S1. Glyceraldehyde 3-phosphate dehydrogenase (GAPDH) was used as an internal control.

2.7. Western blot analysis

Western blot analysis was performed as described previously [22]. An anti-β-actin antibody was used for the normalization of protein expression. Signals were detected using enhanced chemiluminescence (Meilunbio, Dalian, China). The primary antibodies used in this study are listed in Table S2.

2.8. Immunohistochemistry

Immunohistochemistry (IHC) and haematoxylin and eosin (HE) staining were performed as described previously [22]. The primary antibodies used for IHC are listed in Table S2.

2.9. Transmission electron microscopy

The treated cells were centrifuged and immediately fixed in 2.5% phosphate-glutaraldehyde for 4 h. After 2 washes with dimethylarsenic acid sodium buffer, the samples were directly dehydrated in an ethanol gradient, fixed, embedded, and sectioned. The samples were then viewed using a Tecnai 10 (100 kV) transmission electron microscope. For each sample, five fields of view were randomly selected, and 20 mitochondria in each field of view were examined.

2.10. Small interfering RNA transfection

The small interfering RNAs (siRNAs) of target genes and negative siRNA controls were transfected as described previously [22]. Additional information about the siRNAs is provided in Table S3.

2.11. Plasmid construction and transfection

PCR-amplified human wild-type HDLBP, YTH N6-methyladenosine RNA binding protein 2 (YTHDF2), FSP1, and TRIM69 transcripts were cloned into GV141-Flag, GV141-HA or GV141-Myc vectors. The ubiquitin (Ub) sequence was cloned into the GV141-His vector. The deletion mutants and site-specific mutants in our study were generated according to the manufacturer's instructions (GeneChem, Shanghai, China). All reagents used for the experiments described in this section were purchased from GeneChem (Shanghai, China). Transfection was performed as described previously [22].

2.12. Lentivirus construction and infection

Recombinant lentiviruses were obtained by inserting the target gene between the *Age*I and *Eco*RI loci of the GV308 vector. Recombinant lentiviruses were amplified in 293T cells, purified by centrifugation and used for subsequent analysis. The virus titres were determined by fluorescence and drug screening, and recombinant viruses were stored in virus preservation solution at −80 °C. Western blot analysis of infected 293T cells confirmed the existence of lentiviral target products. A lentivirus containing the empty vector GV308 was constructed as a control. The recombinant lentiviruses were stably transfected into the indicated HCC cell lines according to the manufacturer's instructions. The screening drug puromycin was added 72 h after infection, and its concentration was maintained at 5 μg/mL for 24 h. The cells were cultured in this medium for 48 h, and additional assays were then performed. All reagents used for the experiments described in this section were purchased from GeneChem (Shanghai, China).

2.13. Biotinylated-RNA pull-down assay

RNA pull-down was performed using the Pierce Magnetic RNA–-Protein Pull-Down Kit (Thermo Fisher Scientific, 20164) according to the manufacturer's instructions. The cells were washed with PBS and then briefly vortexed in lysis buffer (20 mM Tris-HCl pH 7.5, 0.5% NP-40, 250 mM NaCl, 3 mM EDTA, 3 mM EGTA, 1 mM DTT, 1 mM cocktail, 1 mM PhosphoSTOP, 1 mM NEM, and 1 mm NAM) on ice for 10 min. The lysate was preclarified by centrifugation, and 50 μL of the sample was dispensed for input. The remaining lysate was incubated with streptavidin magnetic beads. An equal volume of 1X RNA Capture Buffer was then added, and the beads were resuspended by pipetting or vortexing. Biotin-labelled RNA (50 pmol) was then added to the beads. The solution was gently mixed by pipetting and then incubated with the cell lysates for 20 min at 30 °C. After incubation, the beads were precipitated by centrifugation at 1000 rpm for 3 min, washed twice with NP40 buffer and washed twice with high-salt NP40 buffer (350 mM NaCl). The proteins bound to the target RNA were eluted by heating the beads with 30 μL of SDS loading buffer at 95 °C for 10 min. The extracted cell lysates were further subjected to mass spectrometry (MS) analysis (Novogene, Tianjin, China) or Western blot analysis. The following biotinylated probes were used in this study: lncFAL, CGAACCAAGATCTGATAGCA-/3bio/; pre-lncFAL, GGGTATGAAAGCAACCTGGA-/3bio/. The antisense RNA or lncΔFAL was used as the negative control, and the extracted protein was used as the positive control.

2.14. RNA immunoprecipitation (RIP)

RIP was performed using the Magna RIPTM RNA-Binding Protein Immunoprecipitation Kit (Merck Millipore, 17–700, Darmstadt, Germany) according to the manufacturer's instructions. In short, cells were crosslinked and lysed with RIP lysis buffer (1 mM DTT, 1 × protease inhibitor, and 1 × RNase inhibitor). Extracts were collected and incubated overnight with primary antibody and Manga ChIP protein A/G magnetic beads at 4 °C. The beads were washed three times with RIP wash buffer. The beads were then resuspended in 150 μL of proteinase K buffer (117 μL of RIP wash buffer, 15 μL of 10% SDS, and 18 μL of 10 mg/mL proteinase K) and incubated for 1 h at 65 °C. The beads were then washed again three times with RIP wash buffer. Phenol:chloroform: isoamyl alcohol (400 μL) was subsequently added to each tube. The samples were vortexed for 15 s and centrifuged at 14000 rpm and room temperature for 10 min to separate the phases. Next, 350 μL of the aqueous phase was carefully removed, and 50 μL of Salt Solution I, 15 μL of Salt Solution II, 5 μL of Precipitate Enhancer, and 850 μL of absolute ethanol were added. The sample was incubated at −80 °C overnight to precipitate the RNA. The purified RNA was then used for qRT−PCR. The antibodies used in the RIP experiments are listed in Table S2. The rabbit IgG antibody isotype control was used as a negative control, and total RNA served as the input control.

2.15. Rapid amplification of cDNA ends (RACE) and Northern blotting

The 5'/3′ RACE Kit (Merck Millipore, 03353621001, Darmstadt, Germany) was used according to the manufacturer's instructions to perform 3′ and 5′ RACE. RNA was extracted from the PLC5 cell line using TRIzol reagent, treated with DNase I (Invitrogen) for first-strand cDNA synthesis, and used for 5′-RACE and 3′-RACE PCRs. The following primers for 3′ and 5′ RACE were designed: AACAGAGGGTATGAAAGCAACCT (First-round lncFAL 3′-prime specific) and CTCTGCACAGGCACACTCC (second-round lncFAL 3′-prime specific); CAGTCGTAGAAGGGGTACTGGTAG (first-round lncFAL 5′-prime specific) and AGTCGTAGAAGGGGTACTGGTAGG (second-round lncFAL 5′-

prime specific). The PCR fragments were purified and cloned into the pDrive TA cloning vector (Qiagen), and the insert with correct sequences as analysed by sequencing was then subcloned into the expression vector plasmids for expression in cells.

We obtained 5 μg of total RNA using a FastPure® Cell/Tissue Total RNA Isolation Kit V2 (Vazyme). According to the manufacturer's protocol, RNA imprinting was performed using the NorthernMax Kit (Ambion). The blots were washed and then imaged using a ChemiDoc™ XRS Molecular Imager system (Bio-Rad, USA).

2.16. MeRIP-qPCR

The m6A level of specific RNAs was determined using the Magna MeRIP™ m6A Kit (Merck Millipore, Darmstadt, Germany). Briefly, 500 μg of total RNA was treated with gDNAwiper mix (Vazyme, Nanjing, China), and the concentration was adjusted to 1 μg/μL with nuclease-free water. Chemically fragmented RNA (100 nt) was immunoprecipitated with an anti-m6A antibody (Abcam, ab284130, Cambridge, UK) according to the manufacturer's instructions, and 1/10 of the fragmented RNA was stored as an input control. The m6A enrichment in each sample was calculated by qPCR and normalized to the input.

2.17. RNA fluorescence in situ hybridization (FISH)

For FISH experiments, the cells were grown on coverslips (WHB, WHB-12-CS, Shanghai, China), fixed with 4% paraformaldehyde (Sigma–Aldrich, Darmstadt, Germany) for 15 min, and then permeabilized with 0.1% Triton X-100 (BioFroxx, Guangzhou, China) for 10 min. Subsequently, 30 ng of the 5′-biotinylated probe was denatured at 42 °C overnight and added to the hybridization buffer (2 x SSC, 10% methylamide, and 100 mg/mL dextran sulfate). The cells were incubated for 3 h at 37 °C in a humidified chamber protected from light for hybridization. After three washes with PBS, the samples were blocked with normal goat serum for 1 h at room temperature. HDLBP antibodies were subsequently added, and the cells were incubated overnight at 4 °C. After three washes with PBS, the cells were incubated with the secondary antibody (BosterBio, BA1105, Wuhan, China) in the dark at room temperature for 1 h. DAPI (0.5 mg/mL) was used to stain the nuclei. lncFAL 5′-biotinylated probes were purchased from RiboBio (Guangzhou, China). The sequence of the lncFAL probe was as follows: 5′-TGCCTGCGGGAACAGAGGGTATGAAAGCAA-3'.

2.18. Coimmunoprecipitation (CoIP)

CoIP assays were performed using a CoIP kit (Abs955, Absin, Shanghai, China) according to the manufacturer's recommended protocol. Briefly, the indicated cells were placed in IP lysis buffer (20 mM Tris-HCl pH 7.5, 0.5% NP-40, 250 mM NaCl, 3 mM EDTA, 3 mM EGTA, 1 mM DTT, 1 mM cocktail, 1 mM PhosphoSTOP, 1 mM NEM, and 1 mm NAM). A total of 500 μg of extract was incubated for 4 h with the indicated primary antibody or IgG as a negative control and then with protein A/G-Sepharose beads for 2 h at 4 °C. After extensive PBS washes, the immunoprecipitates were used for subsequent assays. The antibodies used in the CoIP experiments are listed in Table S2.

2.19. Mass spectrometry analysis

For identification of the interacting proteins from the RNA pull-down assay and CoIP assays, immunoprecipitates of the indicated cells were analysed by SDS–PAGE and digested with 10 ng/μL sequencing-grade trypsin (Promega). The protein was eluted using an eluent consisting of 0.1% formic acid and 75% acetonitrile. The eluted protein was then subjected to quality control and qualitatively analysed using a Q Exactive™ HF-X mass spectrometer by Novogene Co., Ltd. (Tianjin, China) to obtain the raw proteome data. The raw protein file was directly imported into Proteome Discoverer 2.2 software for database searching, matching of peptide spectra, and protein quantification.

2.20. Xenograft assay

Six-week-old female BALB/c nude mice were purchased from Byrness Weil Biotechnology Ltd. (Chengdu, China) and housed in a specific pathogen-free environment with a 12-h light/dark cycle and controlled temperature and humidity, and food and water were provided ad libitum. Three million designated treated PLC5 cells were collected and injected subcutaneously into mice. At least 4 mice were used in each group in each experiment. Once the tumours reached a mean volume of 200 mm^3, the mice were treated intraperitoneally with sorafenib every 3 days. The mice were then euthanized at the indicated time after injection. Each tumour was dissected, fixed with 4% formaldehyde, and embedded in paraffin. The tumour growth was monitored weekly by calliper measurements. The formula for calculating the tumour volume was as follows: volume $= 1/2 \times$ longest diameter $\times$ (shortest diameter)^2. All operations on laboratory animals were performed in accordance with the NIH Guide for the Care and Use of Laboratory Animals and were approved by the Animal Care and Use Committee of West China Hospital, Sichuan University (2020351A).

2.21. Statistical analysis

The statistical analyses were performed using SPSS 24.0, and the data are presented as the means ± standard deviations unless otherwise stated. The median expression value of the genes was set as the cut-off value for determining high and low expression. Receiver operating characteristic (ROC) curve analysis was performed to determine the predicted values of the parameters, and the area under the ROC curve (AUC) values were determined. Unpaired t tests were used to perform statistical between-group comparisons. Paired t tests were used to analyse the expression of lncFAL in 30 HCC tissues and paired adjacent NCL tissues. The chi-square test was used to analyse the clinical correlation between gene expression and clinicopathological features. The Kaplan–Meier method was used to estimate the survival rates, and the log-rank test was used to assess the differences between survival curves. The significant prognostic factors identified in the univariate analysis were further analysed in a multivariate manner using a Cox proportional risk regression model. All *in vitro* experiments and assays were repeated at least three independent times ($N \geq 3$). A P value < 0.05 was considered to indicate statistical significance.

3. Results

3.1. Elevated HDLBP expression is associated with decreased vulnerability to ferroptosis in HCC

A comprehensive analysis of TCGA-LIHC and GEO datasets revealed that few missense mutations of unknown function in the HDLBP gene were observed in HCC patients (3/363, Fig. S1A), but the mRNA expression of HDLBP was markedly elevated in HCC compared with NCL tissues (Fig. 1A) and was significantly upregulated in early-stage HCC tissues (Fig. S1B). Our clinical samples also suggested that HDLBP protein expression was markedly increased in HCC tissues compared with paired NCL tissues (Fig. 1B). Moreover, we observed higher HDLBP expression in different HCC cell lines than in normal hepatocytes (Fig. 1C and S1C).

To further explore the potential biological roles of HDLBP in HCC, we performed a GSEA using the TCGA-LIHC dataset to investigate the dysregulated signalling pathways enriched in HCC with abnormal HDLBP expression. Interestingly, the results indicated that multiple ferroptosis-related metabolic signalling pathways [11–13], including ROS metabolism, glutathione metabolism, tyrosine metabolism, and oxidative phosphorylation, were activated (Fig. 1D). Consistent authentication results were also obtained by GSVA (Fig. S1D). Our

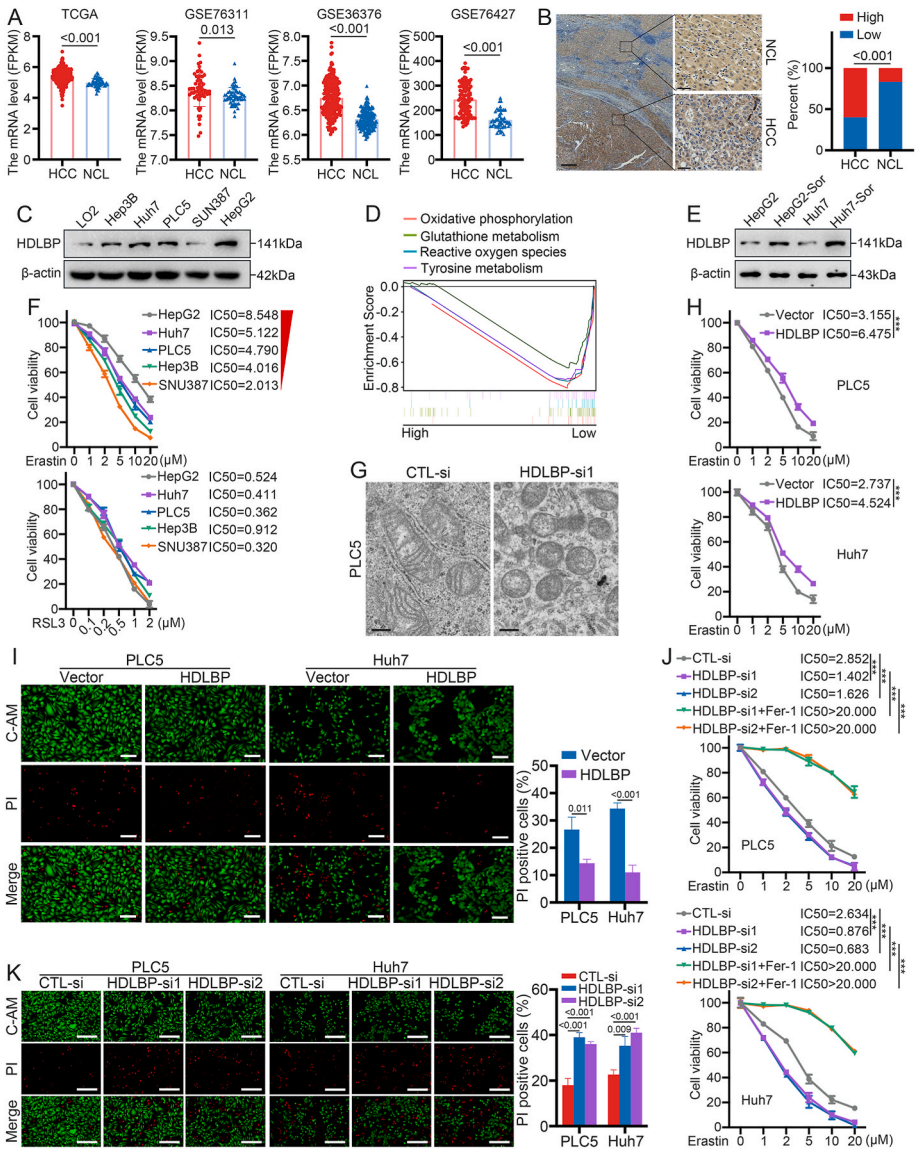

Fig. 1. High HDLBP expression is associated with decreased vulnerability to ferroptosis in HCC. (A) HDLBP expression in hepatocellular carcinoma (HCC) and noncancerous liver (NCL) tissues based on TCGA-LIHC, GSE76311, GSE36376, and GSE76427 datasets. FPKM, fragments per kilobase of exon model per million mapped fragments. (B) Representative images of IHC staining for HDLBP in HCC compared with NCL in our cohort. The right panels (scale bars = 5 μm) show magnified views of the boxed area in the corresponding left panels (scale bars = 5 mm). (C) Western blot analysis of HDLBP protein expression among different HCC cell lines and normal liver cell lines (LO2). β-Actin was used as an internal control. (D) GSEA of HCC patients with different expression levels of HDLBP using TCGA-LIHC data. (E) Western blot analysis of HDLBP protein expression in HCC parental cell lines (Huh7 and HepG2) and sorafenib-adapted cultures of HCC cells (Huh7-Sor and HepG2-Sor, cocultivation for 4 months). β-Actin was used as an internal control. (F) CCK-8 assays of distinct HCC cell lines treated with erastin (1–20 μM) or RSL3 (0.1–2 μM) for 12 h. (G) Representative transmission electron microscopy of PLC5 cells transfected with control siRNA (CTL-si) and HDLBP siRNA1 (HDLBP-si1) and treated with erastin (4 μM) for 12 h. Scale bars = 0.3 μm. (H) CCK-8 assays of PLC5 and Huh7 cells transfected with Flag-control vector (Vector) and Flag-HDLBP overexpression vector (HDLBP) following treatment with erastin (1–20 μM) for 24 h. (I) Calcein-AM/PI staining of PLC5 and Huh7 cells transfected with Vector and HDLBP following treatment with erastin (4 μM) for 24 h. Right panel: relative quantitative analysis of Calcein-AM/PI staining. C-AM, Calcein-AM. Scale bars = 100 μm. (J) CCK-8 assays of PLC5 and Huh7 cells transfected with control siRNA (CTL-si) and HDLBP siRNA (HDLBP-si) following treatment with or without erastin (1–20 μM) and Fer-1 (2 μM) for 24 h. (K) Calcein-AM/PI staining of PLC5 and Huh7 cells transfected with CTL-si and HDLBP-si following treatment with erastin (4 μM) for 24 h. Right panel: relative quantitative analysis of Calcein-AM/PI staining. C-AM, Calcein-AM. Scale bars = 200 μm. All the above experiments were independently performed in triplicate ($N \geq 3$). The data are presented as the means ± SDs. The statistical analyses were performed by two-tailed unpaired Student's *t*-test (A, F, H–K) and the chi-square test (B), respectively.

qRT–PCR results further demonstrated that the expression levels of PTGS2, a marker of ferroptosis, were markedly lower in high HDLBP-expressing HCC than in low HDLBP-expressing HCC (Fig. S1E). Therefore, we speculated that abnormal HDLBP expression is associated with ferroptosis vulnerability in HCC.

Unexpectedly, the ferroptosis inducers erastin and sorafenib did not alter the expression levels of HDLBP within a short duration (Figs. S1F–G), indicating that the occurrence of ferroptosis does not cause the observed variation in HDLBP expression. Conversely, the HDLBP expression levels in HCC were significantly increased after prolonged coculture with sorafenib (Fig. 1E), and consistent results were also obtained from the GEO dataset (Fig. S1H). A previous study showed that ferroptosis vulnerability was significantly reduced after prolonged coculture with sorafenib in HCC [23]. These results revealed that elevated HDLBP expression may be a facilitator of reducing vulnerability to ferroptosis in HCC. Importantly, the vulnerability of various HCC cell lines to erastin but not RSL3 (a GPX4 inhibitor) gradually declined with increasing HDLBP expression (Fig. 1F). Moreover, transmission electron microscopy revealed ferroptosis-like mitochondrial destruction [12], including an obviously increased mitochondrial membrane density, fragmented mitochondrial outer membranes, and disrupted mitochondrial ridges, in HCC cells with low HDLBP expression after erastin treatment (Fig. 1G).

To further demonstrate the association between HDLBP expression and ferroptosis in HCC, we used HCC cells with gain or loss of HDLBP expression to investigate the variations in ferroptosis vulnerability. As expected, ectopic HDLBP expression markedly inhibited erastin-induced cell damage (Fig. 1H–I). Moreover, HDLBP overexpression lessened mitochondrial injury (Fig. S1I) and repressed the erastin-induced increases in the ROS and lipid peroxide levels in HCC cells (Figs. S1J–K). In contrast, the ferroptosis inducer erastin accelerated cell damage in HCC cells with low HDLBP expression (Fig. 1J–K). Moreover, erastin exacerbated mitochondrial injury (Fig. S2A) and rapidly evoked increases in the levels of ROS and lipid peroxides (Figs. S2B–C) in HCC cells with low HDLBP expression. More importantly, erastin-induced damage in HDLBP-silenced HCC cells could be rescued by Fer-1 (a ferroptosis inhibitor) (Fig. 1J and S2D-G) but not by Z-VAD-FMK (a pan-caspase inhibitor) (Figs. S2D–G). In summary, these data indicate that increased HDLBP expression suppresses ferroptosis vulnerability in HCC.

3.2. HDLBP binds to and stabilizes lncFAL in HCC

To further investigate the gene profile alterations accompanying HDLBP overexpression in HCC cells after sorafenib coculture, we performed whole-transcriptome sequencing of parental HCC cell lines (Huh7 and HepG2) and sorafenib-cocultured HCC cells (Huh7-Sor and HepG2-Sor). Because HDLBP has an RNA-binding function, we decided to focus on HDLBP-interacting RNAs, particularly noncoding RNAs. As shown in Fig. 2A, substantially pronounced alterations in lncRNA expression occurred, and these included 602 upregulated and 289 downregulated lncRNAs. We analysed the binding potential of HDLBP with differentially expressed lncRNAs (log |fold change (FC)|>4) using an online lncPro tool (binding coefficient>85) [24] and ultimately identified five lncRNAs. RIP assays further supported NONHSAG111059.1 as a potential downstream lncRNA that binds to HDLBP (Fig. 2A). In this study, NONHSAG111059.1 was renamed lncFAL due to its role as a potential ferroptosis-associated lncRNA (FAL) in HCC.

lncFAL was located on human chromosome 22 and was poorly conserved across species because no clear direct orthologous counterpart could be identified in the mouse genome by Basic Local Alignment Search Tool (BLAST) analysis. The pre-lncFAL transcript in the NONCODE database was NONHSAT244982.1 [25]. By 5′- and 3′- RACE, we discovered that lncFAL is a 636-nt lncRNA (Fig. S3A). According to the open reading frame (ORF) Finder [26], lncFAL has no representative protein-coding ORFs longer than 300 nt. Ribosome profiling suggested the absence of ribosomes on lncFAL [27]. Coding substitution frequencies of lncFAL revealed a low protein-coding potential [28,29]. FISH assays demonstrated that lncFAL localized primarily to the cytoplasm of HCC cells (Fig. 2B), and this finding was verified by qRT–PCR of the nuclear and cytoplasmic fractions (Fig. S3B). Consequently, lncFAL is a lncRNA localized in the cytoplasm of HCC cells. In addition, the NONCODE database implied that lncFAL was only weakly expressed in normal livers but extensively expressed in various cancer cell lines, including HepG2 (Fig. S3C) [25]. More importantly, our qRT–PCR results demonstrated that lncFAL was significantly overexpressed in HCC tissues compared with paired NCL tissues, and the maximal variation was higher than 20-fold (Fig. 2C). lncFAL expression was significantly higher in mid-stage HCC than in early-stage HCC (Fig. S3D). Furthermore, RNA pull-down and RIP assays using various mutant constructs of HDLBP and lncFAL suggested that the KM1-7 domain of HDLBP interacted intensively with the 300-636-nt segment of lncFAL (Fig. 2D–E).

LncRNA homeostasis is maintained by a “production-degradation” balance [30], and HDLBP plays essential roles in maintaining RNA stability [31], which prompted us to further explore whether HDLBP could affect lncFAL stability. As expected, FISH assays implied that the lncFAL levels were affected by the HDLBP protein levels (Fig. S3E), and a quantitative analysis further suggested that lncFAL expression was markedly increased in response to the HDLBP abundance in a dose- and time-dependent manner (Fig. 2F and G). As a control, the HDLBP$^{\Delta KH1\text{-}7}$ deletion mutant did not affect lncFAL expression (Fig. 2G). We then treated HCC cells with ActD, a pan transcriptional inhibitor, and found that lncFAL degradation was inhibited in HDLBP-overexpressing HCC cells (Fig. 2H and S3F), whereas reduction in the HDLBP levels markedly promoted lncFAL degradation (Figs. S3G–H). Furthermore, treating HCC cells with RNasin and DEPC, two pan-RNase inhibitors, restricted the role of reduced HDLBP expression on the lncFAL half-life (Fig. 2I). Overall, these results indicated that HDLBP bound to lncFAL in the cytoplasm of HCC cells and increased lncFAL stability.

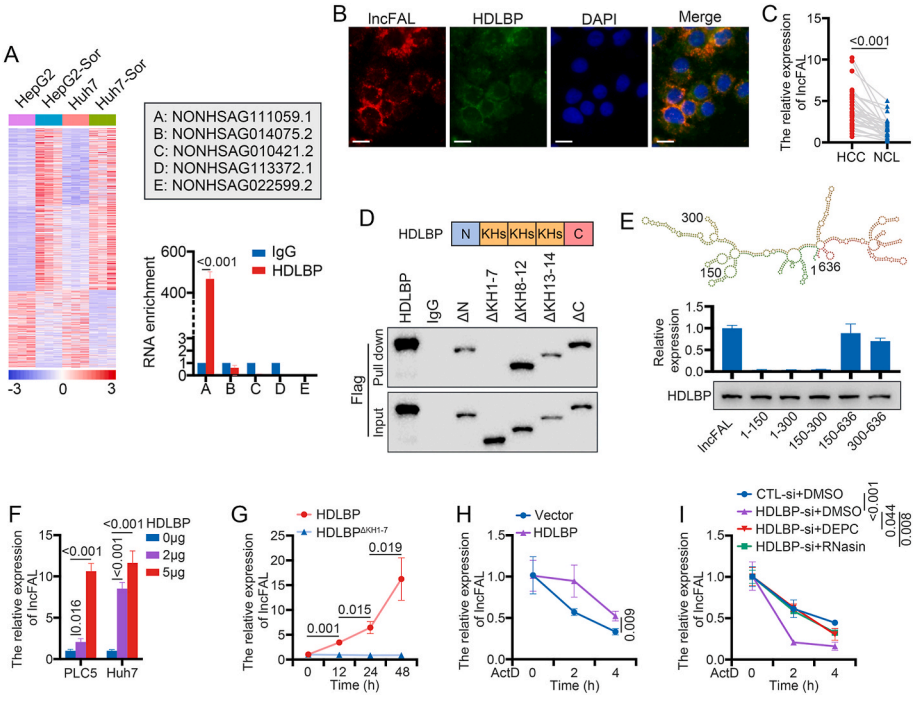

Fig. 2. HDLBP binds to lncFAL and stabilizes its expression. (A) Left panel: Cluster heatmap of differentially expressed lncRNAs between parental cell lines and sorafenib-adapted cultures of HCC cells. Right panel: Potential HDLBP-binding lncRNAs and RNA immunoprecipitation (RIP) results against HDLBP. (B) Fluorescence in situ hybridization (FISH) assays of the expression and location of lncFAL and HDLBP in PLC5 cells. DAPI-stained nuclei are indicated in blue. Scale bars = 1 μm. (C) qRT–PCR analysis of lncFAL expression in HCC compared with NCL. GAPDH was used as an internal control. (D) Upper panel: Schematic diagram of HDLBP protein domains. Lower panel: The interaction between lncFAL and different deletion mutants of HDLBP was assessed by exogenous RNA pull-down assays followed by Western blot analysis. (E) Upper panel: Schematic diagram of the predicted secondary structure of lncFAL. Lower panel: The interaction between HDLBP and different truncated mutants of lncFAL was performed by RIP assays followed by qRT–PCR. (F) qRT–PCR analysis of lncFAL expression in PLC5 and Huh7 cells transfected with different doses of Flag-HDLBP. GAPDH was used as an internal control. (G) qRT–PCR analysis of lncFAL expression in PLC5 cells transfected with Flag-HDLBP and Flag-HDLBP$^{\Delta KH1\text{-}7}$ for the indicated times. GAPDH was used as an internal control. (H) qRT–PCR analysis of lncFAL expression in PLC5 cells transfected with Flag-control vector (Vector) and Flag-HDLBP overexpression vector (HDLBP) and then treated with ActD (5 μg/mL) for the indicated times. GAPDH was used as an internal control. (I) qRT–PCR analysis of lncFAL expression in PLC5 cells transfected with the indicated siRNAs and treated or not treated with DMSO, DEPC, or RNasin (5 U/μL). GAPDH was used as an internal control. All the above experiments were independently performed in triplicate ($N \geq 3$). The data in A and F–I are presented as the means ± SDs. The statistical analyses were performed by two-tailed unpaired Student's *t*-test (A and F–I) and paired Student's *t*-test (C), respectively. (For interpretation of the references to colour in this figure legend, the reader is referred to the Web version of this article.)

3.3. The splicing of lncFAL is increased by YTHDF2 in a m6A-dependent manner in HCC

Using the University of California Santa Cruz (UCSC) Genome Browser, we found that lncFAL originates from the plexin B2 (PLXNB2) gene, which spans an exonic region, and this finding prompted us to query why the lncFAL levels were significantly increased rather than spliced into PLXNB2 mRNA in HCC. Studies have illustrated that m6A methylation is an essential mechanism that regulates mRNA splicing [32]. Coincidentally, an online SRAMP analysis revealed that the pre-lncFAL sequence contains multiple "GGAC" motifs, which are potential m6A modification sites (Fig. 3A) [33]. RNA pull-down was then performed against endogenous PLC5 lysates using the biotinylated pre-lncFAL and lncFAL probes, and this assay was followed by mass spectrometry analysis. Interestingly, we observed that YTHDF2 could visibly bind to pre-lncFAL but not to lncFAL (Table S4). Moreover, the analysis of TCGA and GEO data indicated that YTHDF2 expression was markedly increased in HCC tissues compared with NCL tissues (Fig. 3B and S4A). Consequently, we speculated that the increased expression of YTHDF2 in HCC could promote PLXNB2 premRNA splicing into lncFAL.

As expected, YTHDF2 overexpression significantly increased the expression of lncFAL, whereas the expression of pre-lncFAL was markedly reduced. Moreover, the data showed that the YTH domain was a prerequisite for YTHDF2 to modulate lncFAL expression (Fig. 3C). However, the reduction in PLXNB2 levels suppressed the facilitative effect of YTHDF2 on lncFAL expression (Fig. 3D), and similarly, YTHDF2 knockdown significantly decreased lncFAL expression (Fig. 3E). We further treated HCC cells with ActD and demonstrated that YTHDF2 accelerated pre-lncFAL degradation and markedly increased the lncFAL levels (Fig. 3F and S4B). Moreover, the YTH domain was definitely essential for YTHDF2 to increase lncFAL splicing in HCC (Fig. 3F and S4B). The treatment of HCC cells with DEPC and RNasin also blocked YTHDF2 function (Fig. 3G). Furthermore, EXOSC10 and XRN2 are two major exonucleases responsible for 3′ to 5′ and 5′ to 3′ exonucleolytic activity [34,35], respectively. The deletion of EXOSC10, but not XRN2, abrogated the modulatory effect of YTHDF2 on lncFAL (Fig. 3H), which further indicated that YTHDF2 promoted 3′-5′ pre-lncFAL degradation.

To further confirm the presence of YTHDF2-mediated m6A modification in pre-lncFAL, we performed RIP analysis, which revealed that pre-lncFAL was more abundant than lncFAL in YTHDF2 immunoprecipitates (Fig. 3I). MeRIP-qPCR suggested a significant enrichment of m6A in pre-lncFAL, and the m6A levels in pre-lncFAL were markedly increased after YTHDF2 knockdown (Fig. 3J), which indicated that the m6A level of pre-lncFAL was adversely correlated with the YTHDF2 protein levels. The exact m6A levels of the three potential m6A modification sites shown in Fig. 3A were confirmed by MeRIP-qPCR using

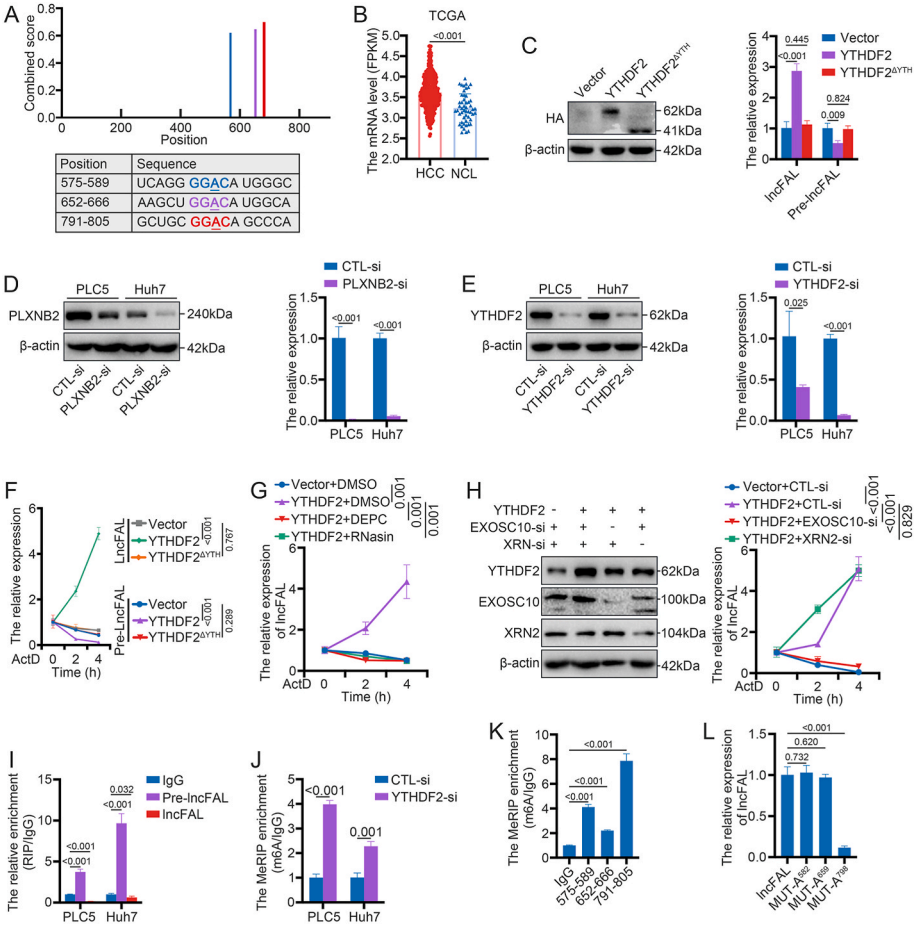

Fig. 3. YTHDF2 regulates the lncFAL expression levels in a m6A-dependent manner. (A) Top sequence motif of m6A methylation sites of pre-lncFAL identified using online SRAMP tools. (B) Expression of YTHDF2 in HCC and NCL tissues from the TCGA-LIHC dataset. (C) Western blot analysis of YTHDF2 protein and qRT–PCR analysis of lncFAL and pre-lncFAL expression in PLC5 cells transfected with HA-control vector, HA-YTHDF2 expression vector, and HA-YTHDF2$^{\Delta YTH}$ expression vector. β-Actin and GAPDH were used as internal controls. (D) Western blot analysis of PLXNB2 protein and qRT–PCR analysis of lncFAL expression in YTHDF2-overexpressing PLC5 and Huh7 cells transfected with CTL-si and PLXNB2-si, respectively. β-Actin and GAPDH were used as internal controls. (E) Western blot analysis of YTHDF2 protein and qRT–PCR analysis of lncFAL expression in PLC5 and Huh7 cells transfected with CTL-si and YTHDF2-si, respectively. β-Actin and GAPDH were used as internal controls. (F) qRT–PCR analysis of lncFAL and pre-lncFAL expression in PLC5 cells transfected with the indicated overexpression vector and then treated with ActD (5 μg/mL) for the indicated times. GAPDH was used as an internal control. (G) qRT–PCR analysis of lncFAL expression in PLC5 cells transfected with the indicated overexpression vectors an treated or not treated with DMSO, DEPC, or RNasin (5 U/μL) treatment following ActD (5 μg/mL) treatment for the indicated times. GAPDH was used as an internal control. (H) Western blot analysis of the indicated proteins and qRT–PCR analysis of lncFAL expression in PLC5 cells transfected with the indicated overexpression vectors and siRNAs and then treated with ActD (5 μg/mL) for the indicated times. β-Actin and GAPDH were used as internal controls. (I) The interaction between YTHDF2 and lncFAL was assessed by RIP assays followed by qRT–PCR. IgG was used as a negative control. (J) MeRIP-qPCR analysis of pre-lncFAL in PLC5 and Huh7 cells transfected with CTL-si and YTHDF2-si, respectively. IgG was used as a negative control. (K) MeRIP-qPCR analysis of the indicated segments of pre-lncFAL in PLC5 cells. IgG was used as a negative control. (L) qRT–PCR analysis of lncFAL expression in PLC5 cells transfected with the indicated overexpression vectors. All the above experiments were independently performed in triplicate (N ≥ 3). The data in B-L are presented as the means ± SDs. The statistical analyses in B-L were performed by the two-tailed unpaired Student's *t*-test.

segmented RNA primers (Fig. 3K). However, the expression of lncFAL was significantly inhibited only after the adenosine (A) at position 798 in the pre-lncFAL sequence was disrupted (Fig. 3L). These results suggested that YTHDF2 could promote lncFAL expression in a m6A-dependent manner in HCC.

3.4. lncFAL modulates HCC ferroptosis vulnerability in vitro and in vivo

We subsequently evaluated whether lncFAL expression was a critical trigger mediating the inhibition of ferroptosis vulnerability by HDLBP in HCC. Although lncFAL overexpression or knockdown failed to elicit alterations in the expression of GPX4 (Fig. S5A), a marker of redox homeostasis, HCC cells overexpressing lncFAL exhibited decreased vulnerability to ferroptosis, including reduced cellular damage (Fig. 4A–B), diminished mitochondrial damage (Fig. S5B) and decreased in ROS accumulation and lipid peroxides (Figs. S5C–D). Conversely, the silencing of lncFAL in HCC cells markedly promoted erastin-mediated ferroptosis (Fig. 4C–G and S5E-F). Moreover, this severe damage was apparently inhibited by Fer-1 (Fig. 4F–H). To further confirm that HDLBP or lncFAL modulates ferroptosis vulnerability independent of GPX4, HCC cells were treated with RSL3. As expected, RSL3-induced ferroptosis was not regulated by lncFAL (Fig. 4I). Consistent with the *in vitro* results, the overexpression of lncFAL markedly restricted the inhibitory effect of sorafenib on the growth of subcutaneous HCC xenografts (Fig. 4J). In contrast, the silencing of lncFAL assisted sorafenib in preventing the subcutaneous growth of HCC cells (Fig. 4K). Notably, the IHC staining of xenograft tumours suggested no significant difference in GPX4 expression in lncFAL-dysregulated HCC (Figs. S5G–H). These results certainly indicated that lncFAL could modulate ferroptosis vulnerability independent of the GPX4 signalling pathway in HCC.

3.5. lncFAL interacts with and inhibits FSP1 degradation

We observed that several genes adjacent to the lncFAL locus, such as MAPK11, MAPK12, and DENND6B, were markedly dysregulated in the TCGA-LIHC dataset (Fig. S6A), but the silencing of lncFAL did not affect the expression of these adjacent genes (Fig. S6B), which indicated that lncFAL might not function as a *cis*-acting gene. Because lncFAL was localized in the cytoplasm, we speculated that lncFAL plays major roles in posttranscriptional regulation. Among the top putative binding proteins of lncFAL (Table S4), FSP1 was recently reported as a novel potential target against ferroptosis independent of the GPX4 signalling

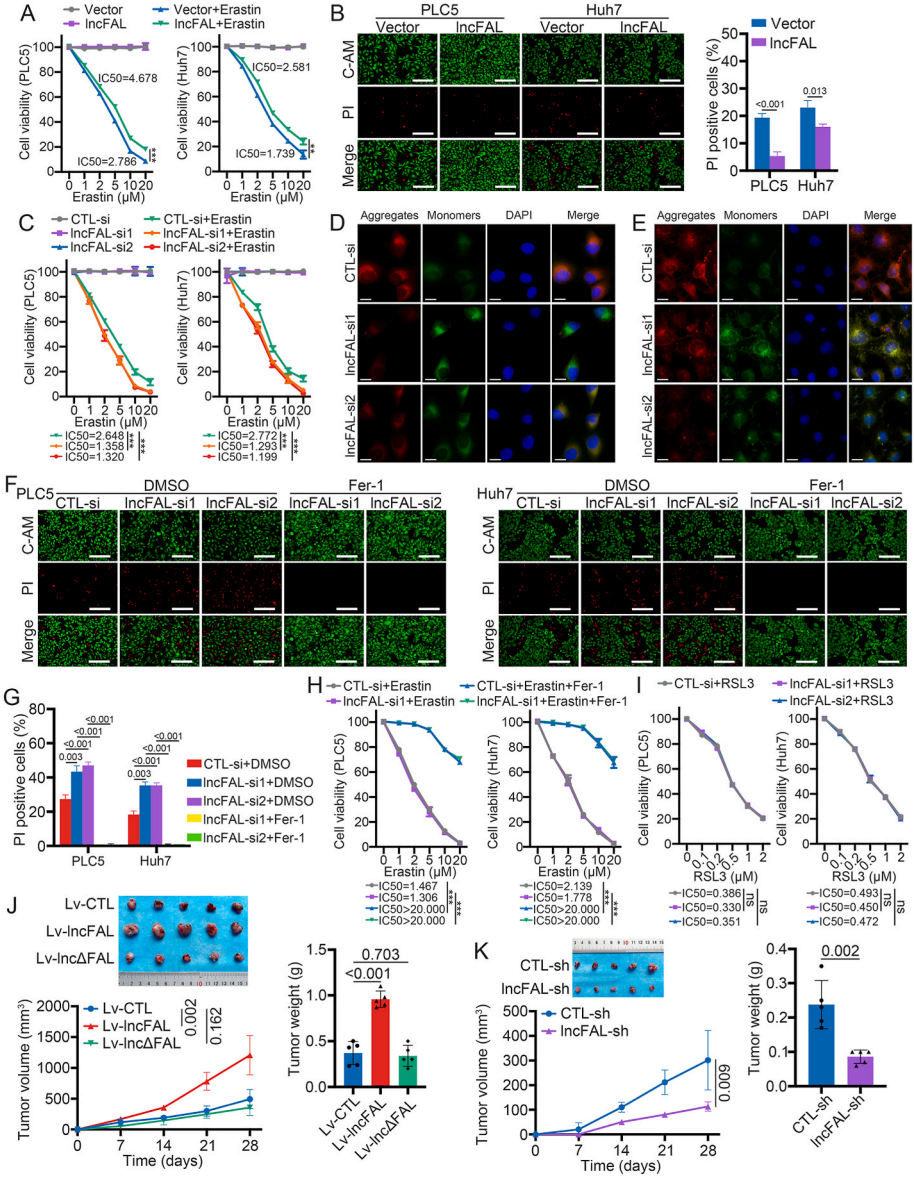

Fig. 4. lncFAL regulates ferroptosis vulnerability in HCC. (A) CCK-8 assays of PLC5 and Huh7 cells transfected with control vector (Vector) and lncFAL overexpression vector (lncFAL) following treatment with erastin (1–20 μM) for 24 h. (B) Calcein-AM/PI staining of PLC5 and Huh7 cells transfected with Vector and lncFAL following treatment with erastin (4 μM) for 24 h. Right panel: relative quantitative analysis of Calcein-AM/PI staining. C-AM, Calcein-AM. Scale bars = 200 μm. (C) CCK-8 assays of PLC5 and Huh7 cells transfected with CTL-si and lncFAL-si following treatment with or without erastin (1–20 μM) for 24 h. (D–E) Representative images of immunofluorescence staining with the JC-1 probe in (D) PLC5 and (E) Huh7 cells transfected with CTL-si and lncFAL-si and treated with erastin (4 μM) for 12 h. Scale bars = 1 μm. (F–G) Calcein-AM/PI staining of PLC5 and Huh7 cells transfected with CTL-si and lncFAL-si following treatment with erastin (4 μM) and with/without Fer-1 (2 μM) for 24 h. C-AM, Calcein-AM. Scale bars = 200 μm. Relative quantitative analysis of Calcein-AM/PI staining (G). (H) CCK-8 assays of PLC5 and Huh7 cells transfected with CTL-si and lncFAL-si following treatment with or without erastin (1–20 μM) and Fer-1 (2 μM) for 24 h. (I) CCK-8 assays of PLC5 and Huh7 cells transfected with CTL-si and lncFAL-si following treatment with RSL3 (0.1–2 μM) for 12 h. (J) Representative images of the xenograft, tumour volume, and tumour weight 28 days after inoculation of PLC5 cells infected with Lv-CTL, Lv-lncFAL, and Lv-lncΔFAL (n = 5 per group). The tumour volumes were measured every 7 days. (K) Representative images of the xenograft, tumour volume, and tumour weight 28 days after inoculation of PLC5 cells infected with CTL-shRNA (CTL-sh) and lncFAL-shRNA (lncFAL-sh) (n = 5 per group). The tumour volumes were measured every 7 days. The experiments in A-H were independently performed in triplicate (N ≥ 3). The data in are presented as the means ± SDs. The statistical analyses were performed by two-tailed unpaired Student's *t*-test (A-C, G-K).

pathway [36], but the tumour-related biological importance of FSP1 in combating ferroptosis is largely unknown. The interaction of lncFAL with FSP1 was identified and validated (Fig. 5A). The specific interaction of FSP1 with the 150-300-nt segment of lncFAL was further recognized by RIP assays (Fig. 5B and S6C). Notably, the mutant lncΔFAL with the 150–636-nt region deleted was unable to bind to FSP1 (Fig. S6C) or to modulate the vulnerability of HCC cells to ferroptosis *in vitro* and *in vivo* (Figs. S6D-E and 4J).

We subsequently verified whether lncFAL regulates FSP1 expression at the posttranscriptional level. As expected, the overexpression of full-length lncFAL, but not lncΔFAL, markedly increased the FSP1 protein levels *in vitro* and *in vivo* (Fig. 5C and S5G) but barely affected the FSP1 mRNA levels (Fig. 5C), and the overexpression of lncFAL increased the FSP1 protein levels in a dose-dependent manner (Fig. 5D). In contrast, the silencing of lncFAL markedly decreased the protein levels (Fig. 5E and S5H) but not the mRNA levels of FSP1 (Fig. S6F). Additionally, the protein level but not the mRNA level of FSP1 was markedly increased in HDLBP-overexpressing HCC cells (Fig. 5F), and the silencing of lncFAL reversed the increase in the FSP1 protein levels induced by HDLBP overexpression (Fig. 5G).

We further used the proteasome inhibitor MG132 to ascertain whether lncFAL affects FSP1 degradation. Interestingly, the overexpression or silencing of lncFAL barely altered the FSP1 protein levels when proteasome-mediated protein degradation was blocked by MG132 in HCC cells regardless of whether HDLBP was overexpressed (Fig. 5G and S6G). Additionally, the overexpression of full-length lncFAL, but not lncΔFAL, increased the half-life of FSP1 protein (Fig. 5H), whereas the silencing of lncFAL significantly facilitated the degradation of FSP1 protein and reversed the impact of HDLBP overexpression on FSP1 stability (Fig. 5I and S6H).

We then sought to determine whether lncFAL inhibited FSP1 degradation by regulating the ubiquitination of FSP1. As expected, the overexpression of FSP1-interactive lncFAL resulted in significant inhibition of K48-linked but not K29-linked or K63-linked polyubiquitination of the FSP1 protein (Fig. 5J–K and S6I-J), whereas the silencing of lncFAL significantly promoted K48-linked polyubiquitination of the FSP1 protein in HCC cells (Fig. 5L and S6K). Furthermore, the polyubiquitination of FSP1 protein was markedly eliminated in HDLBP-overexpressing HCC cells (Fig. S6L), and the silencing of lncFAL robustly reversed the inhibitory effect of HDLBP overexpression on FSP1 polyubiquitination in HCC cells (Fig. 5M). In short, these results reveal that the binding of lncFAL to FSP1 abolishes the polyubiquitination-based degradation of FSP1 protein and thereby increases the FSP1 protein levels.

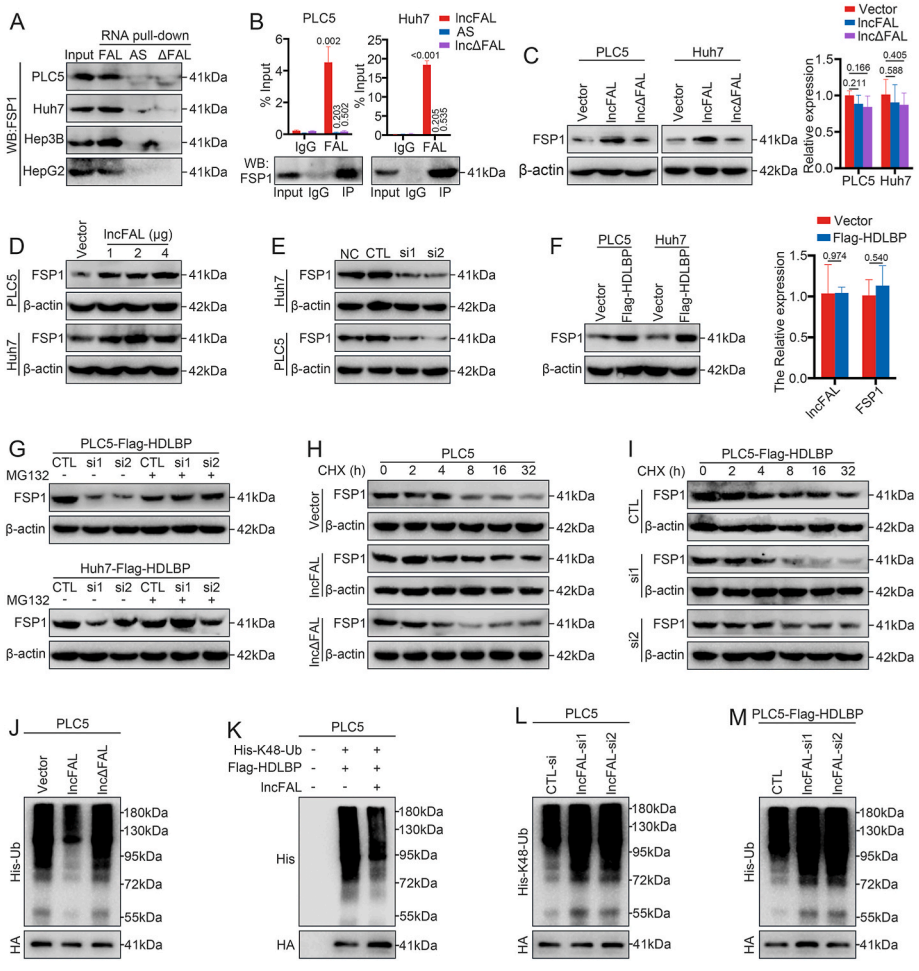

Fig. 5. lncFAL binds to and stabilizes FSP1. (A) RNA pull-down assays validated the interaction between lncFAL (FAL) and FSP1 in the indicated cells. Antisense RNA of lncFAL (AS) and lncΔFAL (ΔFAL) were used as negative controls. (B) RIP assays validated the interaction of FSP1 with lncFAL. Antisense RNA of lncFAL (AS) and lncΔFAL (ΔFAL) were used as negative controls. (C) Western blot analysis of FSP1 protein expression and qRT–PCR analysis of FSP1 mRNA expression in the indicated cells transfected with lncFAL-expressing, lncΔFAL-expressing, or control vectors. β-Actin and GAPDH were used as internal controls. (D) Western blot analysis of FSP1 protein expression in the indicated cells transfected with various doses of lncFAL-expressing or control vector. β-Actin was used as an internal control. (E) Western blot analysis of FSP1 protein expression in the indicated cells transfected with lncFAL-siRNA and CTL-si. NC, normal control. β-Actin was used as an internal control. (F) Western blot analysis of FSP1 protein expression and qRT–PCR analysis of FSP1 mRNA expression in the indicated cells transfected with Flag-HDLBP-expressing or control vector. β-Actin and GAPDH were used as internal controls. (G) Western blot analysis of FSP1 protein expression in the indicated Flag-HDLBP-overexpressing HCC cells transfected with lncFAL-si or CTL-si and treated or not treated with MG132. β-Actin was used as an internal control. (H) Western blot analysis of the effect of lncFAL-expressing, lncΔFAL-expressing, or control vectors on the half-life of FSP1 in PLC5 cells treated with cycloheximide (CHX) for the indicated times. β-Actin was used as an internal control. (I) Western blot analysis of the effect of lncFAL-si or control-si on the half-life of FSP1 in HDLBP-overexpressing PLC5 cells treated with cycloheximide (CHX) for the indicated times. β-Actin was used as an internal control. (J–M) HA-FSP1-overexpressing PLC5 cells were transfected as indicated, and the cell lysates were then immunoprecipitated with anti-HA antibody and detected with anti-His antibody. All the above experiments were independently performed in triplicate ($N \geq 3$). The data in B, C, and F are presented as the means ± SDs. The statistical analyses were performed by the two-tailed unpaired Student's *t*-test (B, C, and F).

3.6. lncFAL disrupts the FSP1-TRIM69 interaction

To further investigate the mechanism of lncFAL-mediated ubiquitination degradation of the FSP1 protein, we screened potential FSP1-binding E3 ligases using the online BioGRID and IntAct tools [37,38]. Here, we noticed TRIM69 because it was previously reported to promote protein polyubiquitination [39]. We then investigated whether Trim69 induced the degradation of FSP1 and whether lncFAL could affect this process in HCC. As expected, we found that Trim69 could indeed interact with FSP1 (Fig. 6A–B) to decrease the FSP1 protein levels through proteasome-mediated degradation (Fig. 6C), which would cause K48-linked FSP1 polyubiquitination (Fig. 6D) and thus shorten the half-life of FSP1 in HCC cells (Fig. 6E), and these findings imply that Trim69 is a critical E3 ligase of FSP1. Importantly, the overexpression of lncFAL decreased the binding of Trim69 to FSP1 in a dose-dependent manner (Fig. 6F). Moreover, the overexpression of lncFAL largely abolished the Trim69-induced K48-linked polyubiquitination of FSP1 protein and thereby increased the FSP1 protein levels (Fig. 6G–H). Furthermore, when Trim69 expression was presilenced in HDLBP-overexpressing HCC cells, the silencing of lncFAL failed to both promote FSP1 polyubiquitination and reduce the FSP1 levels (Fig. 6I–J). These data suggest that lncFAL competitively bound to FSP1 and thereby eliminated the interaction of FSP1 with the E3 ligase Trim69, which leads to disruption of Trim69-dependent degradation of the FSP1 protein.

3.7. FSP1 blockade is essential for HCC therapy

We subsequently investigated whether the Trim69-FSP1 interaction was critical for the ferroptosis-inhibiting role of lncFAL in HCC. We first validated that restoring lncFAL expression reversed the effect of HDLBP silencing on promoting the vulnerability of HCC cells to ferroptosis (Fig. 7A–B and S7A). Notably, after erastin treatment, lncFAL-overexpressing HCC cells in which FSP1 was silenced exhibited more severe cellular damage (Fig. 7C–D), more visible mitochondrial injury (Fig. S7B) and higher ROS and lipid peroxide levels (Figs. S7C–D) than control cells, and importantly, these effects could be reversed by Fer-1 (Fig. 7D–E). Consistent results were also observed with sorafenib-treated HCC cells (Figs. S7E–F). These data indicated that the silencing of FSP1 greatly reversed the inhibitory effect of lncFAL on the vulnerability of HCC to ferroptosis. More importantly, ubiquinol, a downstream antioxidant product of FSP1, significantly inhibited the ferroptosis vulnerability of HDLBP- or lncFAL-silenced HCC cells (Fig. 7F–G), which reveals that HDLBP-stabilized lncFAL indeed acts in trans by inhibiting FSP1 degradation to eliminate ferroptosis vulnerability.

Moreover, the xenograft tumour growth of lncFAL-overexpressing HCC cells in which FSP1 is silenced was also significantly inhibited by sorafenib *in vivo* (Fig. 7H). However, the silencing of lncFAL barely altered the ferroptosis vulnerability of HCC *in vitro* (Figs. S7G–J) and *in vivo* (Figs. S8A–D) when TRIM69 was silenced or FSP1 was reintroduced in HCC cells. The IHC results from *in vivo* assays further demonstrated that lncFAL regulated FSP1 and ferroptosis vulnerability independently of the GPX4 signalling pathway (Fig. 7I and S8C-D). Consistently, the silencing of HDLBP also failed to improve the ferroptosis vulnerability of HCC *in vitro* when TRIM69 was silenced or FSP1 was reintroduced in HCC cells (Figs. S8E–H). Therefore, FSP1 blockade is essential for the promotion of ferroptosis vulnerability in HCC.

3.8. Poor prognosis of HCC patients with high expression of HDLBP or lncFAL

We further analysed the correlations of lncFAL with HDLBP and FSP1 using our HCC samples. As expected, a positive correlation between the lncFAL levels and HDLBP or FSP1 protein expression was obtained in our HCC cohorts (additional details are provided in Table S5). Specifically,

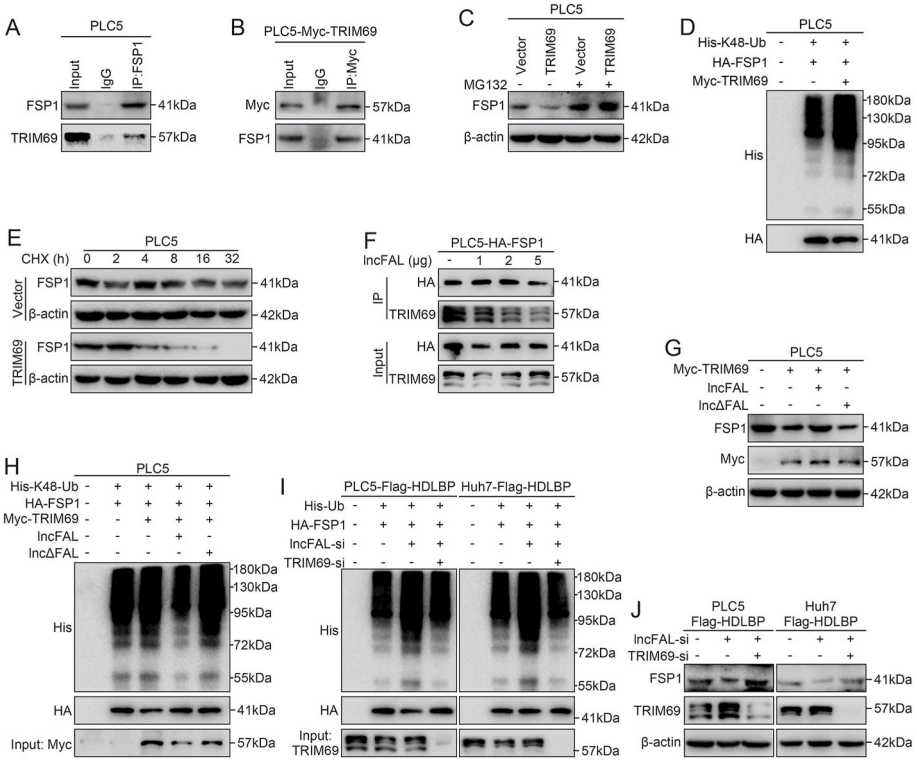

Fig. 6. lncFAL abrogates the Trim69-induced degradation of FSP1. (A) The interaction between FSP1 and Trim69 was assessed by immunoprecipitation assays followed by Western blot analysis. IgG was used as a negative control. (B) The interaction between Myc-tagged TRIM69 and FSP1 was assessed by immunoprecipitation assays followed by Western blot analysis. IgG was used as a negative control. (C) Western blot analysis of FSP1 protein expression in control-vector or Trim16-overexpressing PLC5 cells treated or not treated with MG132. β-Actin was used as an internal control. (D) PLC5 cells were transfected as indicated, and the cell lysates were then immunoprecipitated with anti-HA antibody and detected with anti-His antibody. (E) Western blot analysis of the effect of Trim16 overexpression and the control vector on the half-life of FSP1 in PLC5 cells treated with cycloheximide (CHX) for the indicated times. β-Actin was used as an internal control. (F) The interaction between Trim69 and HA-tagged FSP1 was evaluated by CoIP assays followed by Western blot analysis in PLC5 cells transfected with different doses of lncFAL-overexpressing vector. (G) Western blot analysis of FSP1 protein expression in PLC5 cells transfected with the indicated vectors. β-Actin was used as an internal control. (H–I) The indicated HCC cells were transfected as indicated, and the cell lysates were then immunoprecipitated with anti-HA antibody and detected with anti-His antibody. (J) Western blot analysis of FSP1 protein expression in PLC5- or Huh7-Flag-HDLBP cells in which lncFAL was silenced or Trim69 was knocked down. β-Actin was used as an internal control. All the above experiments were independently performed in triplicate (N ≥ 3).

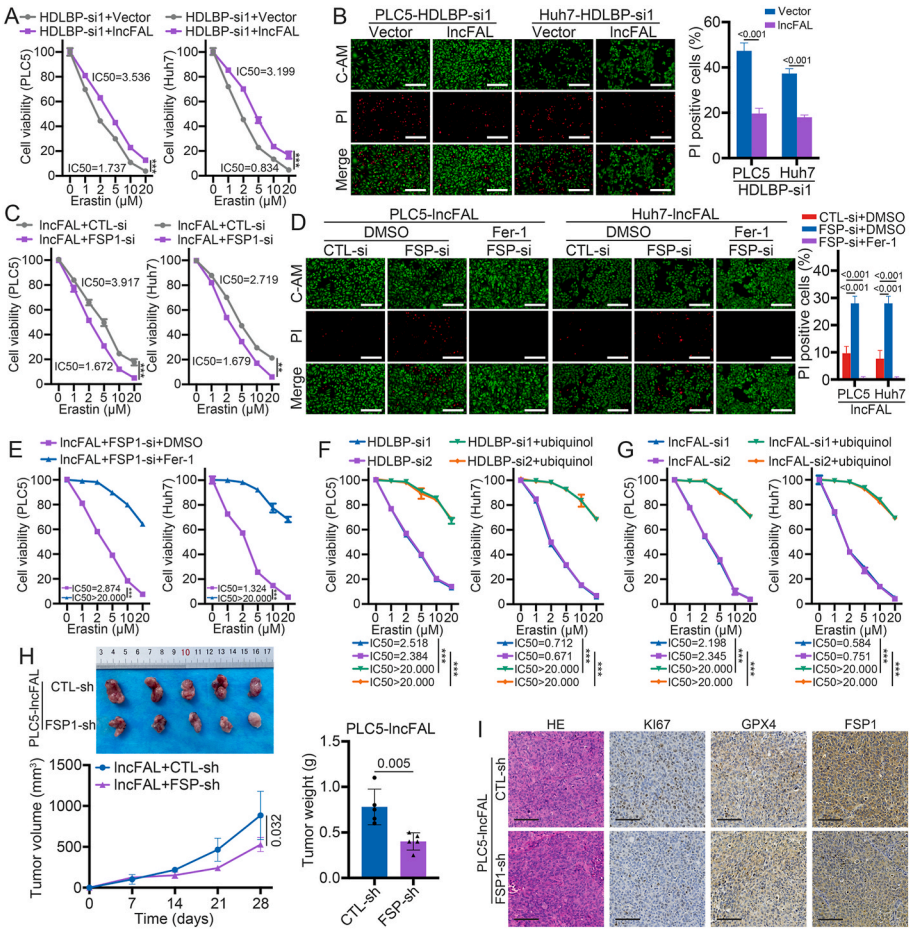

Fig. 7. FSP1 blockade is crucial for ferroptosis vulnerability in HCC. (A) CCK-8 assays of HDLBP silenced HCC cells transfected with control vector (Vector) and LncFAL expression vector (LncFAL) following treatment with erastin (1–20 μM) for 24 h. (B) Calcein-AM/PI staining of HDLBP silenced HCC cells transfected with Vector and lncFAL following treatment with erastin (4 μM) for 24 h. Right panel: relative quantitative analysis of Calcein-AM/PI staining. C-AM, Calcein-AM. Scale bars = 200 μm. (C) CCK-8 assays of lncFAL-overexpressing HCC cells transfected with FSP-si or CTL-si following treatment with erastin (1–20 μM) for 24 h. (D) Calcein-AM/PI staining of lncFAL-overexpressing HCC cells transfected with FSP-si or CTL-si following treatment with erastin (4 μM) and with/without Fer-1 (2 μM) for 24 h. (E) CCK-8 assays of lncFAL-overexpressing HCC cells transfected with FSP1-si following treatment with erastin (1–20 μM) and with/without Fer-1 (2 μM) for 24 h. (F) CCK-8 assays of HDLBP silenced HCC cells treated with erastin (1–20 μM) and with/without ubiquinol (1 μg) for 24 h. (G) CCK-8 assays of lncFAL silenced HCC cells treated with erastin (1–20 μM) and with/without ubiquinol (1 μg) for 24 h. (H) Representative images of the xenograft, tumour volume and tumour weight 28 days after inoculation of lncFAL-overexpressing PLC5 cells infected with FSP-sh or CTL-sh (n = 5 per group). The tumour volumes were measured every 7 days. (I) Representative images of HE and IHC of Ki67, GPX4, and FSP1 expression in the implanted HCC tumours in each group. Scale bars = 50 μm. The experiments in A-G were independently performed in triplicate (N ≥ 3). The data are presented as the means ± SDs. The statistical analyses were performed by the two-tailed unpaired Student's *t*-test (A–H).

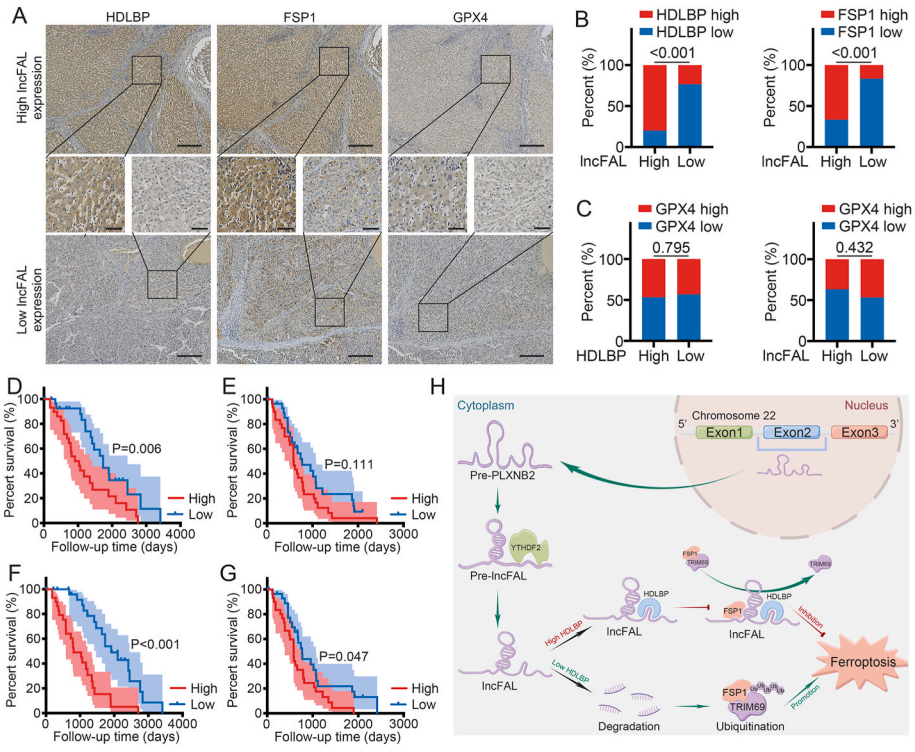

Fig. 8. The HDLBP and lncFAL expression levels are significantly associated with prognosis in HCC. (A) Representative IHC images of HDLBP, FSP1, and GPX4 expression in 60 HCC tissues. The middle panels (scale bars = 50 μm) show magnified views of the boxed area in the corresponding upper or lower panels (scale bars = 200 μm). (B) Correlations between lncFAL and HDLBP or FSP1 expression levels. (C) Correlations of HDLBP and lncFAL with the GPX4 expression levels. The statistical analyses in B–C were performed by the chi-square test. The (D) overall survival (OS) and (E) recurrence-free survival (RFS) of HCC patients with different HDLBP protein expression levels were assessed by Kaplan–Meier survival curves and log-rank tests. The (F) OS and (G) RFS of HCC patients with different lncFAL expression levels were assessed by Kaplan–Meier survival curves and log-rank tests. (H) Schematic showing the regulation of ferroptosis vulnerability in HCC by HDLBP, which stabilizes PLXNB2-derived lncFAL. This effect enhanced the binding of lncFAL to its target FSP1, diminished the Trim69-dependent degradation of FSP1, and thereby inhibited ferroptosis vulnerability in HCC. Conversely, the inhibition of HDLBP or lncFAL expression contributed to the promotion of ferroptosis in HCC.

80.00% and 66.67% of the HCC tissues with high lncFAL expression exhibited high HDLBP and FSP1 protein expression, respectively. Moreover, 76.67% and 83.33% of HCC tissues with low lncFAL levels presented low levels of HDLBP and FSP1 protein expression (Fig. 8A–B), respectively, which further supported the role of HDLBP-stabilized lncFAL in promoting tumour resistance to ferroptosis via FSP1 during HCC treatment. However, the IHC results of our cohort suggested that the lncFAL levels or HDLBP protein expression were indeed not obviously correlated with GPX4 (Fig. 8C).

We further found that lncFAL expression had better diagnostic value than HDLBP, with an AUC of 75.00% (Fig. S9). More importantly, our analysis revealed that high HDLBP or lncFAL expression correlated with an advanced BCLC stage, advanced AJCC stage, larger tumour size, poorer tissue differentiation, and higher serum AFP levels (Table S5). Kaplan–Meier analysis suggested that the OS of HCC patients with high HDLBP expression was significantly worse than that of patients with low HDLBP expression (Fig. 8D), whereas recurrence-free survival (RFS) was not significantly different regardless of HDLBP expression (Fig. 8E). Moreover, HCC patients with high lncFAL expression had significantly poorer OS and RFS than HCC patients with low lncFAL expression (Fig. 8F–G). An univariate analysis demonstrated that high HDLBP expression, high lncFAL expression, advanced BCLC stage, advanced AJCC stage, larger tumour size, poorer tissue differentiation and microvascular invasion were unfavourable predictors of the OS of HCC patients (Table S6). Further multivariate analysis showed that lncFAL was an independent prognostic factor of the OS of HCC patients (Table S7).

4. Discussion

Metabolic abnormalities are one of the major biological features of malignancy and can comprehensively affect the biological behaviours of tumours, such as tumour growth, proliferation, and metastasis [40]. Although the roles of many metabolic molecules or products in tumours have been investigated after years of dedicated studies [41], few metabolic factors could be used as effective therapeutic targets for HCC. Therefore, there is an urgent need to explore whether aberrant metabolic signatures could be clinically applicable therapeutic targets. Lipids are mainly processed in the liver and play an essential role in the physiology of this organ and in the pathological progression of HCC [42]. The role of HDLBP, as one of the critical lipid transport proteins in the liver [43], has been scarcely explored in tumour progression. Tang et al. only reported that HDLBP was associated with malignant growth in HCC [20]. Our study not only reveals that HDLBP is a crucial suppressor of ferroptosis vulnerability in HCC but also demonstrates that HDLBP-stabilized lncFAL exerts a regulatory effect on ferroptosis vulnerability by blocking the degradation of the FSP1 protein.

Similar to protein regulators, increasing evidence indicates that lncRNAs play an essential role in modulating the malignant biological behaviour of tumours and have enormous potential for clinical applications in the diagnosis and treatment of cancer [44]. When exploring the potential mechanisms of HDLBP, the largest RNA-binding protein [19], in HCC, we sought to identify ncRNAs that bind to HDLBP but have not yet been characterized, and we ultimately settled on lncFAL. In addition to a large number of alternative transcription start sites and termination and splicing patterns, new antisense, intronic and intergenic transcripts of lncRNAs have been identified in recent years [45]. Interestingly, our analysis of the lncFAL sequence revealed that lncFAL originated from an exonic region of the PLXNB2 gene. After further investigation, we found that YTHDF2 overexpression in HCC facilitated PLXNB2 premRNA splicing into lncFAL in a m6A-dependent manner, which partially explained the marked increase in lncFAL in HCC. More importantly, our study suggested that HDLBP directly bound to lncFAL and inhibited its degradation in HCC and thereby the sensitivity of HCC cells to erastin or sorafenib. Moreover, clinical data indicated that high lncFAL levels or HDLBP levels were associated with a poor prognosis in HCC patients. These data support the potential of HDLBP and lncFAL as therapeutic targets or prognostic markers for HCC patients.

Studies have suggested that redox imbalance and abnormal iron metabolism are two pivotal factors triggering ferroptosis [46]. When ferroptosis was initially reported, researchers attributed this process to the failure of GPX4 and impaired intracellular lipid oxidation, which leads to the accumulation of ROS on membrane lipids catalysed by iron ions and results in an intracellular redox imbalance and the induction of cell death [47]. However, in 2019, Doll et al. published a study demonstrating that the FSP1-CoQ10-NAD(P)H pathway regulates ferroptosis in a manner independent of GPX4 signalling [48]. Interestingly, Dai et al. further found that FSP1 blocks ferroptosis independent of CoQ10/ubiquinol metabolism [49]. Notably, erastin directly binds VDAC2 and causes mitochondrial damage by generating ROS in a NADH-dependent manner, which results in the induction of cellular ferroptosis [11–13]. In parallel, RSL3 binds and inactivates GPX4 and thus mediates ferroptosis regulated by GPX4 inhibition [50]. Interestingly, our current study revealed that HDLBP protein expression in different HCC cell lines was markedly positively correlated with erastin sensitivity but not with RSL3 sensitivity. Moreover, our data indicated that HDLBP or lncFAL could modulate erastin- and sorafenib-induced but not RSL3-induced ferroptosis. Moreover, the promotion of ferroptosis sensitivity after HDLBP or lncFAL knockdown could be reversed by ubiquinol. These data fully demonstrate that HDLBP-stabilized lncFAL regulates ferroptosis vulnerability through FSP1/CoQ10/ubiquinol metabolism but independent of GPX4 signalling. Furthermore, mechanistically, the binding of lncFAL to FSP1 competitively abolishes Trim69-induced polyubiquitination and thereby attenuates FSP1 degradation. These findings may contribute to a better understanding of the mechanism of FSP1-related tumour resistance to ferroptosis and imply that modulation of FSP1 protein is a potential therapeutic approach for HCC.

In conclusion, our study not only elucidates the mechanism through which HDLBP overexpression abrogates TRIM69-dependent FSP1 degradation by stabilizing lncFAL in HCC (Fig. 8H) but also provides a foundation for the establishment of therapeutic strategies aimed at modulating FSP1 stability for the systemic treatment of HCC.

Author contributions

JYY, YS, and LY conceived the project and supervised and designed the entire research study. TL and JY designed and conducted the bioinformatic analysis. TL, JY and JSY were involved in the collection of the clinical samples and clinical data. JSY, TL and JY performed the RIP, RNA pulldown, MeRIP-qPCR and CoIP assays. JSY and TL performed the cytology experiments. TL, ZW and JSY designed and performed the mouse experiments. YS supervised the *in vivo* studies. JSY and ZW performed the Western blot, IHC and qRT−PCR analyses. YS and JSY performed the data analyses. JYY, YS, LY and JSY wrote the manuscript.

Funding

This work was supported by grants from the National Natural Science Foundation of China (no. 82070674), the Sichuan Province Science and Technology Department Project (no. 2019YFG0036), the 1.3.5 Project for Disciplines of Excellence, West China Hospital, Sichuan University (no. ZY2017308), the 1.3.5 Project for Disciplines of Excellence, West China Hospital, Sichuan University (2020HXFH010 to Y. S. and ZYJC1808).

Ethics statement

The study using clinical samples was approved by the Ethics Committee on Biomedical Research, West China Hospital of Sichuan University (2016, no. 120). Informed consent was obtained from all patients or their relatives. All operations of experimental animals were

performed in accordance with the National Institutes of Health's Guide for the Care and Use of Laboratory Animals. All operations were approved by the Animal Care and Use Committee of West China Hospital of Sichuan University (2020351A).

Declaration of competing interest

None.

Data availability

Data will be made available on request.

Acknowledgements

We are most grateful for West China Biobanks, Department of Clinical Research Management, West China Hospital, Sichuan University for their support of human tissue samples.

Appendix A. Supplementary data

Supplementary data to this article can be found online at https://doi.org/10.1016/j.redox.2022.102546.

References

[1] N. Fujiwara, S.L. Friedman, N. Goossens, Y. Hoshida, Risk factors and prevention of hepatocellular carcinoma in the era of precision medicine, J. Hepatol. 68 (2018) 526–549.
[2] P. Konyn, A. Ahmed, D. Kim, Current epidemiology in hepatocellular carcinoma, Expet Rev. Gastroenterol. Hepatol. 15 (2021) 1295–1307.
[3] H. Sung, J. Ferlay, R.L. Siegel, M. Laversanne, I. Soerjomataram, A. Jemal, F. Bray, Global Cancer Statistics 2020: GLOBOCAN estimates of incidence and mortality worldwide for 36 cancers in 185 countries, CA, Cancer J. Clin. 71 (2021) 209–249.
[4] M. Reig, A. Forner, J. Rimola, J. Ferrer-Fàbrega, M. Burrel, Á, Garcia-Criado, R. K. Kelley, P.R. Galle, V. Mazzaferro, R. Salem, B. Sangro, A.G. Singal, A. Vogel, J. Fuster, C. Ayuso, J. Bruix, BCLC strategy for prognosis prediction and treatment recommendation: the 2022 update, J. Hepatol. 76 (2022) 681–693.
[5] C.H. Zhang, M. Li, Y.P. Lin, Q. Gao, Systemic therapy for hepatocellular carcinoma: advances and hopes, Curr. Gene Ther. 20 (2022) 84–99.
[6] J.M. Llovet, S. Ricci, V. Mazzaferro, P. Hilgard, E. Gane, J.F. Blanc, A.C. de Oliveira, A. Santoro A, J.L. Raoul, A. Forner, M. Schwartz, C. Porta, S. Zeuzem, L. Bolondi, T.F. Greten, P.R. Galle, J.F. Seitz, I. Borbath, D. Häussinger, T. Giannaris, M. Shan, M. Moscovici, D. Voliotis, J. Bruix, SHARP Investigators Study Group, Sorafenib in advanced hepatocellular carcinoma, N. Engl. J. Med. 359 (2008) 378–390.
[7] J. Awosika, D. Sohal, A narrative review of systemic treatment options for hepatocellular carcinoma: state of the art review, J. Gastrointest. Oncol. 13 (2022) 426–437.
[8] P.R. Galle, F. Tovoli, F. Foerster, M.A. Wörns, A. Cucchetti, L. Bolondi, The treatment of intermediate stage tumours beyond TACE: from surgery to systemic therapy, J. Hepatol. 67 (2017) 173–183.
[9] E. Harding-Theobald, J. Louissaint, B. Maraj, E. Cuaresma, W. Townsend, M. Mendiratta-Lala, A.G. Singal, G.L. Su, A.S. Lok, N.D. Parikh, Systematic review: radiomics for the diagnosis and prognosis of hepatocellular carcinoma, Aliment. Pharmacol. Ther. 54 (2021) 890–901.
[10] A.L. Cheng, C. Hsu, S.L. Chan, S.P. Choo, M. Kudo, Challenges of combination therapy with immune checkpoint inhibitors for hepatocellular carcinoma, J. Hepatol. 72 (2020) 307–319.
[11] M.M. Capelletti, H. Manceau, H. Puy, K. Peoc'h, Ferroptosis in liver diseases: an overview, Int. J. Mol. Sci. 21 (2020) 4908.
[12] X. Chen, C. Yu, R. Kang, G. Kroemer, D. Tang, Cellular degradation systems in ferroptosis, Cell Death Differ. 28 (2021) 1135–1148.
[13] Y. Chen, Z. Fan, S. Hu, C. Lu, Y. Xiang, S. Liao, Ferroptosis: a new strategy for cancer therapy, Front. Oncol. 12 (2022), 830561.
[14] R. Kong, N. Wang, W. Han, W. Bao, J. Lu, IFNγ-mediated repression of system xc- drives vulnerability to induced ferroptosis in hepatocellular carcinoma cells, J. Leukoc. Biol. 110 (2021) 301–314.
[15] Y. Su, B. Zhao, L. Zhou, Z. Zhang, Y. Shen, H. Lv, L.H.H. AlQudsy, P. Shang, Ferroptosis, a novel pharmacological mechanism of anti-cancer drugs, Cancer Lett. 483 (2020) 127–136.
[16] P. Tang, J. Sheng, X. Peng, R. Zhang, T. Xu, J. Hu, Y. Kang, B. Wu, H. Dang, Targeting NOX4 disrupts the resistance of papillary thyroid carcinoma to chemotherapeutic drugs and lenvatinib, Cell Death Dis. 8 (2022) 177.
[17] O.F. Kuzu, M.A. Noory, G.P. Robertson, The role of cholesterol in cancer, Cancer Res. 76 (2016) 2063–2070.
[18] G. Kroemer, J. Pouyssegur, Tumor cell metabolism: cancer's Achilles' heel, Cancer Cell 13 (2008) 472–482.
[19] M.H. Cheng, R.P. Jansen, A Jack of All Trades: the RNA-Binding Protein Vigilin, vol. 8, Wiley Interdiscip. Rev. RNA, 2017.
[20] W.L. Yang, L. Wei, W.Q. Huang, R. Li, W.Y. Shen, J.Y. Liu, J.M. Xu, B. Li, Y. Qin, Vigilin is overexpressed in hepatocellular carcinoma and is required for HCC cell proliferation and tumor growth, Oncol. Rep. 31 (2014) 2328–2334.
[21] Y. Zhou, H. Ji H, Q. Xu, X. Zhang, X. Cao, Y. Chen, M. Shao, Z. Wu, J. Zhang, C. Lu, J. Yang, Y. Shi, H. Bu, Congenital biliary atresia is correlated with disrupted cell junctions and polarity caused by Cdc42 insufficiency in the liver, Theranostics 11 (2021) 7262–7275.
[22] J. Yuan, Z. Yin, L. Tan, W. Zhu, K. Tao, G. Wang, W. Shi, J. Gao, Interferon regulatory factor-1 reverses chemoresistance by downregulating the expression of P-glycoprotein in gastric cancer, Cancer Lett. 457 (2019) 28–39.
[23] R. Gao, R.K.R. Kalathur, M. Coto-Llerena, C. Ercan, D. Buechel, S. Shuang, S. Piscuoglio, M.T. Dill, F.D. Camargo, G. Christofori, F. Tang, YAP/TAZ and ATF4 drive resistance to Sorafenib in hepatocellular carcinoma by preventing ferroptosis, EMBO Mol. Med. 13 (2021), e14351.
[24] C.M. Mann, U.K. Muppirala, D. Dobbs, Computational prediction of RNA-protein interactions, Methods Mol. Biol. 1543 (2017) 169–185.
[25] L. Zhao, J. Wang, Y. Li, T. Song, Y. Wu, S. Fang S, D. Bu, H. Li, L. Sun, D. Pei, Y. Zheng, J. Huang, M. Xu, R. Chen, Y. Zhao, S. He, NONCODEV6: an updated database dedicated to long non-coding RNA annotation in both animals and plants, Nucleic Acids Res. 49 (2021) D165–D171.
[26] E.W. Sayers, E.E. Bolton, J.R. Brister, K. Canese, J. Chan, D.C. Comeau, R. Connor, K. Funk, C. Kelly, S. Kim, T. Madej, A. Marchler-Bauer, C. Lanczycki, S. Lathrop, Z. Lu, F. Thibaud-Nissen, T. Murphy, L. Phan, Y. Skripchenko, T. Tse, J. Wang, R. Williams, B.W. Trawick, K.D. Pruitt, S.T. Sherry, Database resources of the national center for biotechnology information, Nucleic Acids Res. 50 (2022) D20–D26.
[27] N.T. Ingolia, G.A. Brar, S. Rouskin, A.M. McGeachy, J.S. Weissman, The ribosome profiling strategy for monitoring translation in vivo by deep sequencing of ribosome-protected mRNA fragments, Nat. Protoc. 7 (2012) 1534–1550.
[28] T. Hung, Y. Wang, M.F. Lin, A.K. Koegel, Y. Kotake Y, G.D. Grant GD, H. M. Horlings, N. Shah, C. Umbricht, P. Wang, Y. Wang, B. Kong, A. Langerød, A. L. Børresen-Dale, S.K. Kim, M. van de Vijver, S. Sukumar, M.L. Whitfield, M. Kellis, Y. Xiong, D.J. Wong, H.Y. Chang, Extensive and coordinated transcription of noncoding RNAs within cell-cycle promoters, Nat. Genet. 43 (2011) 621–629.
[29] M.F. Lin, I. Jungreis, M. Kellis, PhyloCSF: a comparative genomics method to distinguish protein coding and non-coding regions, Bioinformatics 27 (2011) i275–i282.
[30] J.B. Pierce, H. Zhou, V. Simion, M.W. Feinberg, Long noncoding RNAs as therapeutic targets, Adv. Exp. Med. Biol. 1363 (2022) 161–175.
[31] X. Yu, Q. Liu, J. He, Y. Huang, L. Jiang, X. Xie, J. Liu, L. Chen, L. Wei, Y. Qin, Vigilin interacts with CTCF and is involved in the maintenance of imprinting of IGF2 through a novel RNA-mediated mechanism, Int. J. Biol. Macromol. 108 (2018) 515–522.
[32] L. Liu, H. Li, D. Hu, Y. Wang, W. Shao, J. Zhong, S. Yang, J. Liu, J. Zhang, Insights into N6-methyladenosine and programmed cell death in cancer, Mol. Cancer 21 (2022) 32.
[33] S. Lin, J. Choe, P. Du, R. Triboulet, R.I. Gregory, The m(6)A methyltransferase METTL3 promotes translation in human cancer cells, Mol. Cell 62 (2016) 335–345.
[34] I. Stuparević, A. Novačić, A.R. Rahmouni, A. Fernandez, N. Lamb, M. Primig, Regulation of the conserved 3'-5' exoribonuclease EXOSC10/Rrp6 during cell division, development and cancer, Biol. Rev. Camb. Phil. Soc. 96 (2021) 1092–1113.
[35] V.K. Nagarajan, C.I. Jones, S.F. Newbury, P.J. Green, XRN 5'→3' exoribonucleases: structure, mechanisms and functions, Biochim. Biophys. Acta 1829 (2013) 590–603.
[36] K. Bersuker, J.M. Hendricks, Z. Li, L. Magtanong, B. Ford, P.H. Tang, M.A. Roberts, B. Tong, T.J. Maimone, R. Zoncu, M.C. Bassik, D.K. Nomura, S.J. Dixon, J. A. Olzmann, The CoQ oxidoreductase FSP1 acts parallel to GPX4 to inhibit ferroptosis, Nature 575 (2019) 688–692.
[37] R. Oughtred, J. Rust, C. Chang, B.J. Breitkreutz, C. Stark, A. Willems, L. Boucher, G. Leung, N. Kolas, F. Zhang, S. Dolma, J. Coulombe-Huntington, A. Chatr-Aryamontri, K. Dolinski, M. Tyers, The BioGRID database: a comprehensive biomedical resource of curated protein, genetic, and chemical interactions, Protein Sci. 30 (2021) 187–200.
[38] S. Orchard, M. Ammari, B. Aranda, L. Breuza, L. Briganti, F. Broackes-Carter, N. H. Campbell, G. Chavali, C. Chen, N. del-Toro, M. Duesbury, M. Dumousseau, E. Galeota, U. Hinz, M. Iannuccelli, S. Jagannathan, R. Jimenez, J. Khadake, A. Lagreid, L. Licata, R.C. Lovering, B. Meldal, A.N. Melidoni, M. Milagros, D. Peluso, L. Perfetto, P. Porras, A. Raghunath, S. Ricard-Blum, B. Roechert, A. Stutz, M. Tognolli, K. van Roey, G. Cesareni, H. Hermjakob, The MIntAct project–IntAct as a common curation platform for 11 molecular interaction databases, Nucleic Acids Res. 42 (2014) D358–D363.
[39] T. Bagga, N.K. Tulsian, Y.K. Mok, R.M. Kini, J. Sivaraman, Mapping of molecular interactions between human E3 ligase TRIM69 and Dengue virus NS3 protease using hydrogen-deuterium exchange mass spectrometry, Cell. Mol. Life Sci. 79 (2022) 233.
[40] D. Hanahan, R.A. Weinberg, Hallmarks of cancer: the next generation, Cell 144 (2011) 646–674.
[41] P.E. Porporato, N. Filigheddu, J.M.B. Pedro, G. Kroemer, L. Galluzzi, Mitochondrial metabolism and cancer, Cell Res. 28 (2018) 265–280.
[42] M. Alannan, H. Fayyad-Kazan, V. Trézéguet, A. Merched, Targeting lipid metabolism in liver cancer, Biochemistry 59 (2020) 3951–3964.
[43] S.A. Wu, S. Kersten, L. Qi, Lipoprotein lipase and its regulators: an unfolding story, Trends Endocrinol. Metabol. 32 (2021) 48–61.

[44] A. Bhan, M. Soleimani, S.S. Mandal, Long noncoding RNA and cancer: a new paradigm, Cancer Res. 77 (2017) 3965–3981.
[45] S. Kong, M. Tao, X. Shen, S. Ju, Translatable circRNAs and lncRNAs: driving mechanisms and functions of their translation products, Cancer Lett. 483 (2020) 59–65.
[46] X. Chen, J. Li, R. Kang, D.J. Klionsky, D. Tang, Ferroptosis: machinery and regulation, Autophagy 17 (2021) 2054–2081.
[47] S.J. Dixon, B.R. Stockwell, The role of iron and reactive oxygen species in cell death, Nat. Chem. Biol. 10 (2014) 9–17.
[48] S. Doll, F.P. Freitas, R. Shah, M. Aldrovandi, M.C. da Silva, I. Ingold, A. Goya Grocin, T.N. Xavier da Silva, E. Panzilius, C.H. Scheel, A. Mourão, K. Buday, M. Sato, J. Wanninger, T. Vignane, V. Mohana, M. Rehberg, A. Flatley, A. Schepers, A. Kurz, D. White, M. Sauer, M. Sattler, E.W. Tate, W. Schmitz, A. Schulze, V. O'Donnell, B. Proneth, G.M. Popowicz, D.A. Pratt, J.P.F. Angeli, M. Conrad, FSP1 is a glutathione-independent ferroptosis suppressor, Nature 575 (2019) 693–698.
[49] E. Dai, W. Zhang, D. Cong, R. Kang, J. Wang, D. Tang, AIFM2 blocks ferroptosis independent of ubiquinol metabolism, Biochem. Biophys. Res. Commun. 523 (2020) 966–971.
[50] X. Sui, R. Zhang, S. Liu, T. Duan, L. Zhai, M. Zhang, X. Han, Y. Xiang, X. Huang, H. Lin, T. Xie, RSL3 drives ferroptosis through GPX4 inactivation and ROS production in colorectal cancer, Front. Pharmacol. 9 (2018) 1371.